

# REVIEW OF MULTIMUON PRODUCTION BY MUONS

Mark Strovink

Physics Department and Lawrence Berkeley Laboratory  
University of California  
Berkeley, California 94720 USA

## ABSTRACT

Production of 2, 3, 4, and 5-muon final states by high-energy muons at Fermilab and CERN SPS is reviewed. Sixty-three  $4\mu$ ,  $5\mu$ , and odd-sign  $3\mu$  final states have been observed. Corresponding limits on muoproduction of  $T$ ,  $b\bar{b}$ , and  $\bar{M}^0$  are summarized. Precise data on the  $Q^2$  and  $\nu$ -dependence of muoproduced elastic- $\psi$ , inelastic- $\psi$ , and open-charm states are presented. Elastic and inelastic  $\psi$  muoproduction results are extended to include distributions in production and decay angle, elasticity, and momentum transfer to hadrons. Calculations using the lowest-order photon-gluon-fusion graph can be adjusted to reproduce the  $\nu$ -dependence of elastic  $\psi$  production, the  $\nu$  and  $Q^2$  dependence of open charm production, and the combined (hidden + open) charm production cross section. Unfortunately, the model does not account for the angular distributions and  $Q^2$ -dependence observed for elastic  $\psi$  production. Unless inhibited by order-of-magnitude threshold effects, the "intrinsic charm" model predicts more copious open charm production at Bjorken  $x=0.4$  than is observed. Inelastic  $\psi$  production exhibits half the  $p_{\perp}^2$  slope observed for elastic  $\psi$  production, with more similar dependence on  $Q^2$  and  $\nu$ . Shapes of the inelastic- $\psi$  distributions in  $\nu$  and elasticity strongly favor calculations which use next-to-lowest-order photon-gluon diagrams explicitly conserving color and C-parity, when compared to those which do not. However, the favored diagrams account for only 18% of the observed cross section.

## INTRODUCTION

The experimental input<sup>1-17</sup> to this review is listed in Table I. I shall emphasize new results, mainly from the Berkeley-Fermilab-Princeton<sup>1</sup> (BFP) and European Muon Collaboration<sup>3</sup> experiments, also including data from the Bologna-CERN-Dubna-Munich-Saclay<sup>4</sup> (BCDMS) and Fermilab-Illinois<sup>9</sup> groups. Most of the data arise from intense ( $10^6$ - $10^8$ Hz) muon bombardment of massive ( $3$ - $10$  kg/cm<sup>2</sup>) nuclear targets, producing final states in which only the muons are fully reconstructed. The resulting high luminosities stimulate searches for new physics in rare final states, to which Section I is devoted. Copious production of  $J/\psi(3100)$  and of open-charm states is observed by means of their decay into muons. I shall discuss mechanisms for elastic  $\psi$  production, open-charm production, and inelastic  $\psi$  production in Sections II, III, and IV. The order is

Table I. Experimental input to this review. New results are below the dashed lines.

| Topic                                 | Authors                       | Group    | Ref | Subtopic   |
|---------------------------------------|-------------------------------|----------|-----|--|
| Rare processes                        | A.R. Clark <u>et al.</u>      | BFP      | 1   | T limit  |
|                                       | A.R. Clark <u>et al.</u>      | BFP      | 2   | $\bar{M}^0$ limit  |
|                                       | — — — —                       |          |     |  |
|                                       | J.J. Aubert <u>et al.</u>     | EMC      | 3   | Exotic $3\mu$  |
|                                       | D. Bollini <u>et al.</u>      | BCMS     | 4   | T limit  |
|                                       | W.H. Smith <u>et al.</u>      | BFP      | 5   | T, $b\bar{b}$ , $\bar{M}^0$ limits;<br>$4\mu$ , $5\mu$ , exotic $3\mu$ |
| J/ $\psi$ elastic                     | A.R. Clark <u>et al.</u>      | BFP      | 6   | $\sigma$ ; $\nu$ , $Q^2$ -dep.   |
|                                       | J.J. Aubert <u>et al.</u>     | EMC      | 7   | $\sigma$ ; $\nu$ , $Q^2$ -dep.   |
|                                       | A.R. Clark <u>et al.</u>      | BFP      | 8   | $\psi$ polarization; $Q^2$ -dep.                                       |
|                                       | — — — —                       |          |     |  |
|                                       | M. Binkley <u>et al.</u>      | FNAL-Il1 | 9   | $\gamma$ (p or D) $\rightarrow$ ( $\psi$ or $\psi'$ ) X                |
|                                       | T.W. Markiewicz <u>et al.</u> | BFP      | 10  | Final results, QCD fits  |
| Open charm ( $c\rightarrow\mu\nu X$ ) | J.J. Aubert <u>et al.</u>     | EMC      | 11  | $2\mu$ cut cross-sections  |
|                                       | J.J. Aubert <u>et al.</u>     | EMC      | 12  | $3\mu$ cut cross-sections  |
|                                       | A.R. Clark <u>et al.</u>      | BFP      | 13  | $2\mu$ $\gamma$ , $\mu$ cross-sections                                 |
|                                       | A.R. Clark <u>et al.</u>      | BFP      | 14  | $2\mu$ structure functions   |
|                                       | G.D. Gollin <u>et al.</u>     | BFP      | 15  | $2\mu$ results, analysis details                                       |
|                                       | — — — —                       |          |     |  |
|                                       | (privately communicated)EMC   |          | 16  | $2\mu$ , $3\mu$ cross-sections,<br>structure functions                 |
| J/ $\psi$ inelastic                   | J.J. Aubert <u>et al.</u>     | EMC      | 17  | Preliminary results  |
|                                       | — — — —                       |          |     |  |
|                                       | T.W. Markiewicz <u>et al.</u> | BFP      | 10  | Final results, QCD fits  |

historical; it also reflects progress in the believability of the QCD-inspired models for these processes, and of the reliability with which they may be tested by experiment.

## I. RARE PROCESSES

### I.1 Limits on $T$ Muoproduction

Dimuon invariant-mass spectra from 102678 fully-reconstructed trimuon final states<sup>1</sup>, and from 637 final states<sup>4</sup> in which two muons are reconstructed, are shown in Figs. 1 and 2, respectively. Figure 1 contains 2 candidates in the  $T$  region with  $1.8 \pm 1.0$  fitted background events; Fig. 2(b) contains 27 candidates in the  $T$  region with 34 calculated background events. As is obvious in the latter figure, the same calculation overestimates the observed lower-mass continuum. Its authors correspondingly increase their estimate of the  $T$  signal, to  $0 \pm \sqrt{27}$  events. The resulting 90%-confidence limits are  $\sigma_B < 22(13) \times 10^{-39} \text{ cm}^2$  at  $\langle E_\mu \rangle = 209(280) \text{ GeV}$ . These do not seriously conflict with vector meson dominance (VMD) and photon-gluon fusion ( $\gamma\text{GF}$ ) predictions, summarized in Ref. 1, which are of the same order.

### I.2 $4\mu$ , $5\mu$ , and Odd-sign $3\mu$ Final States

Tables II and III list sixty of these rare final states observed<sup>5</sup> in the BFP apparatus, and three observed<sup>3</sup> in the EMC apparatus. Also listed are principal backgrounds and estimates of their contributed signal. Primarily, the  $5\mu$  and elastic  $4\mu$  events are second-order radiative corrections to QED muon tridents; inelastic  $4\mu$  events are second-order radiative corrections to charm production with single  $c \rightarrow \mu X$  decay; and the (36) BFP odd-sign trimuons are  $\pi$  or  $K$  decay accompanied by charm production with single  $c \rightarrow \mu X$  decay.

Identification of background mechanisms is aided by kinematic comparisons with the supposed parent sample. For the BFP (EMC) data, these parent samples comprise 188 275 (10 035) dimuons and 110 626 (31 184) trimuons. Figure 3 shows (36) BFP odd-sign trimuons, analyzed (when appropriate) as dimuons, compared to the parent dimuon sample in six variables. Figure 4 exhibits the  $p_T$  distribution of individual muons from (3) EMC odd-sign trimuons. One event, responsible for the three highest values of  $p_T$  in Fig. 4, possesses kinematics which are unusual by the standards of Fig. 3. It is interpreted<sup>3</sup> as a candidate for  $b\bar{b}$  production with a  $(\bar{b} \rightarrow \mu^+; b \rightarrow c \rightarrow \mu^+)$  decay cascade. The corresponding 90%-confidence limit is  $\sigma(\mu N \rightarrow B\bar{B}X) < 12 \times 10^{-36} \text{ cm}^2$  at 250 GeV. A comparable limit ( $17 \times 10^{-36} \text{ cm}^2$  at 209 GeV) has been obtained<sup>5</sup> using (relatively involved) kinematic analysis of BFP dimuon data. These limits do conflict with several VMD- and  $\gamma\text{GF}$ -based predictions (Table IV), while leaving others unthreatened; details may be found in Refs. 3 and 5.

### I.3 Summary

Table IV summarizes the limits on rare processes which have been obtained using muoproduced multimMuon final states. [It includes the published<sup>2</sup> BFP limit

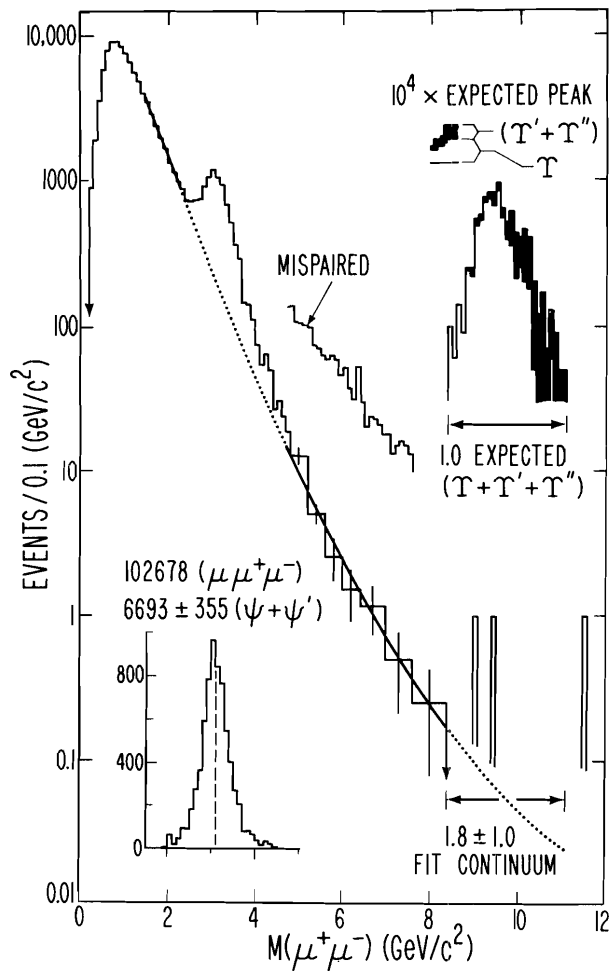


Fig. 1. Spectrum of 102 678 dimuon masses from BFP trimuon data. The background is fitted by  $\exp(a+bM+cM^2)$  in the regions of the solid curve with a  $\chi^2$  of 13.7 for 14 degrees of freedom, and is extrapolated along the dotted curve. The "mispaired" histogram segment illustrates the appearance of the mass spectrum if the alternative muon-pairing choice is made. The background-subtracted  $\psi$  peak is shown in the lower corner; the expected peak from  $10^4$  times the Monte Carlo-simulated  $T$ ,  $T'$ , and  $T''$  sample is shown in the upper corner, with the contribution from  $T'$  and  $T''$  in black.

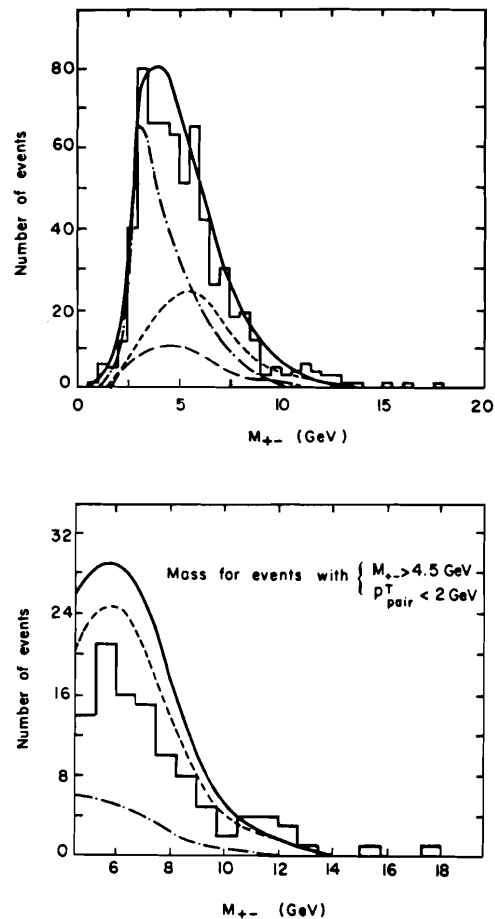


Fig. 2. Spectra of 637 dimuon masses from BCDMS data (the third muon is undetected). The long-dashed, short-dashed, dot-dashed, and solid lines are calculations, respectively, for  $\pi$  and  $K$  decays, QED tridents, bound and unbound charm, and the sum. Because of limited acceptance the  $\psi$  peak is unresolved. The lower distribution, with additional cuts indicated, is interpreted as containing fewer than 7  $T$ 's between 8 and 12  $\text{GeV}/c^2$ .

Table II. Rare events in BFP data (W.H. Smith *et al.*, Ref. 5)

| Type  | No. obs.               | Principal background process  | No. bkgnd expected                 |
|---|------------------------|---|------------------------------------|
| $\mu^\pm N \rightarrow \mu^\pm \mu^\pm \mu^\pm X$         | 8                      | $\mu N \rightarrow \mu c \bar{c} X$ ; $c$ or $\bar{c} \rightarrow \mu^\pm \nu X$ ;<br>third $\mu^\pm$ from $\pi$ or $K$ decay                   | } 18-53 or<br>} 39-45<br>(2 ests.) |
| $\mu^\pm N \rightarrow \mu^\pm \mu^\mp \mu^\mp X$         | <u>28</u><br>36        |   |                                    |
| $\mu^\pm N \rightarrow \mu^\pm \mu^+ \mu^- X$             | 3                      | } QED, e.g.<br>} (one muon may be<br>} too soft to see)   | } $\approx 6-13$                   |
| $\mu^\pm N \rightarrow \mu^\pm \mu^+ \mu^- \mu^+ \mu^- X$ | <u>5</u>               |   |                                    |
| $E_X < 6$ GeV   | 8                      |   |                                    |
| $\mu^\pm N \rightarrow \mu^\pm \mu^+ \mu^- \mu^+ \mu^- X$ | 5                      | inelastic QED, e.g.   | $\approx 2$                        |
| $E_X > 6$ GeV   |                        |   |                                    |
| $\mu^\pm N \rightarrow \mu^\pm \mu^+ \mu^- \mu X$         | 11                     | $\mu N \rightarrow \mu c \bar{c} X$ ; $c$ or $\bar{c} \rightarrow \mu \nu X$ ;<br>internal bremsstrahlung of $\gamma^* \rightarrow \mu^+ \mu^-$ | $\approx 7-13$                     |
| $\mu^\pm N \rightarrow \mu^\pm \mu X$                     | 188275 (parent sample) |   |                                    |
| $\mu^\pm N \rightarrow \mu^\pm \mu^+ \mu^- X$             | 110626 (parent sample) |   |                                    |

Table III. Rare events in EMC data (J.J. Aubert *et al.*, Ref. 3)

| Type                                      | No. obs.              | Principal background process  | No. bkgnd expected |
|---|-----------------------|---|--------------------|
| $\mu^+ N \rightarrow \mu^+ \mu^+ \mu^+ X$ | 2                     | $\mu N \rightarrow \mu c \bar{c} X$ ; $c$ or $\bar{c} \rightarrow \mu^\pm \nu X$ ;<br>third $\mu^\pm$ from $\pi$ or $K$ decay | 0.9                |
| $\mu^+ N \rightarrow \mu^+ \mu^- \mu^- X$ | <u>1</u><br>3         |   |                    |
| $\mu^+ N \rightarrow \mu^+ \mu^\pm X$     | 10035 (parent sample) |   |                    |
| $\mu^+ N \rightarrow \mu^+ \mu^+ \mu^- X$ | 31184 (parent sample) |   |                    |

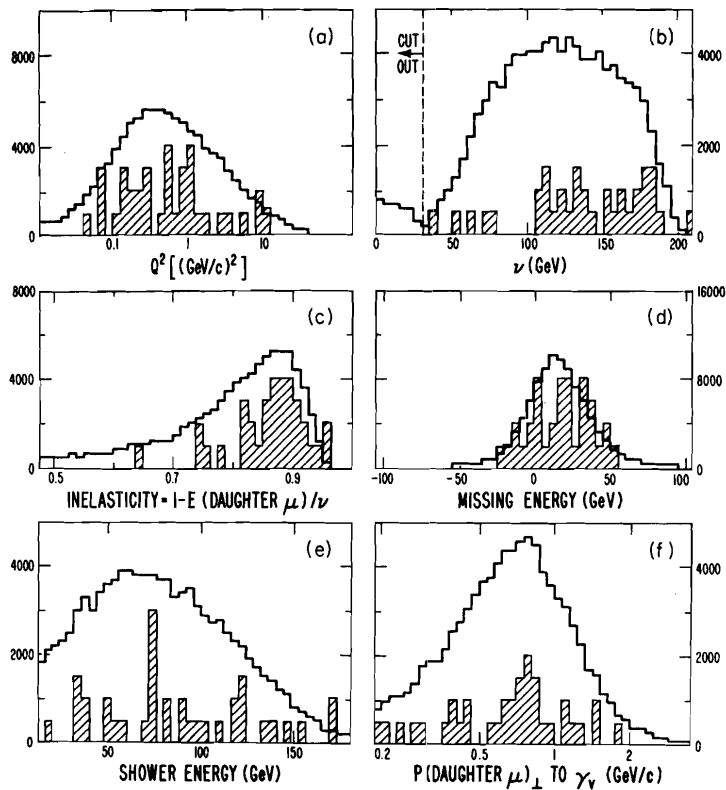


Fig. 3. Distributions (BFP data) in six variables for inelastic dimuons (solid lines) and 36 odd-sign trimuons (hatched blocks, one per event). In distributions (a), (b), and (f), the latter are analyzed as dimuons, with the softest muon ignored. Calculated  $\pi^-$  and  $K^-$  decay background has been subtracted from the dimuons. The distributions are consistent except for  $\nu$  and inelasticity, which are affected by the extra energy required to produce the third muon.

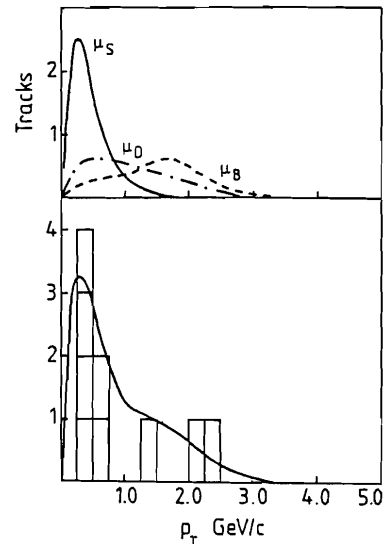


Fig. 4. Distribution (EMC data) in  $p_T$  ( $\perp$  to beam) for 3 odd-sign trimuons. The three highest  $p_T$  muons come from the same event. Dashed, dot-dashed, and solid curves above are calculated spectra from B decay, D decay, and  $\mu^+$  scattering in the process  $\mu^+N \rightarrow \mu^+B\bar{B}X$ ,  $\bar{B} \rightarrow \mu^+X$ ,  $B \rightarrow DX$ ,  $D \rightarrow \mu^+X$ ; the solid curve below is their sum. The calculated background from non-beauty processes is 0.9 events.

Table IV. Limits on muoproduced final states.

| Process   | Group | Ref         | Limit (90% conf)                               | $E_\mu$ (GeV) |
|---|-------|-------------|--|---------------|
| $\mu N \rightarrow \mu TX;$                       | BFP   | 1           | $\sigma_B < 22 \times 10^{-39} \text{ cm}^2$   | 209           |
| $T \rightarrow \mu^+ \mu^-$                       | BCDMS | 4           | 13   | 280           |
|   |       | VMD         | 2-5  | 209           |
| Predictions:                                      |       | VMD         | 4-10   | 280           |
|   |       | $\gamma$ GF | 4-11   | 209           |
|   |       | $\gamma$ GF | 8-22   | 280           |
| $\mu N \rightarrow \mu B\bar{B}X;$                | BFP   | 5           | $\sigma < 17 \times 10^{-36} \text{ cm}^2$     | 209           |
| $(-)$<br>$B \rightarrow \mu \nu X$                | EMC   | 3           | 12   | 250           |
|   |       | VMD         | 4-500  | 209           |
| Predictions:                                      |       | VMD         | 8-1000   | 280           |
|   |       | $\gamma$ GF | 1-60   | 209           |
|   |       | $\gamma$ GF | 2-120  | 280           |
| $\mu N \rightarrow \bar{M}^0 X;$                  | BFP   | 2           | $M_{M^0} \geq 9 \text{ GeV}/c^2$               | 209           |
| $\bar{M}^0 \rightarrow \mu^+ \mu^- \bar{\nu}_\mu$ |       |             | (if RH coupling with Fermi strength, $B=0.1$ ) |               |

on the mass of a heavy neutral muon  $\bar{M}^0$ : if coupled to muons with a right-handed weak current of Fermi strength,  $M_{M^0} > 9 \text{ GeV}/c^2$ , assuming  $B(\bar{M}^0 \rightarrow \mu^+ \mu^- \bar{\nu}_\mu) = 0.1$ . Unfortunately, compelling evidence for new (or even 'beauty') physics has not yet emerged. A single odd-sign  $3\mu$  event (and also single  $4\mu$  and  $5\mu$  events<sup>5</sup>) with unusual kinematics have been identified, along with many such events with more routine kinematics. Fully convincing rejection of background and quantitative physical interpretation demand more than one event.

II. ELASTIC  $\psi$  MUOPRODUCTIONII.1 Background

The muoproduction data<sup>6-8,10</sup> identify  $\psi$ 's by the invariant mass of their decay  $\mu^+\mu^-$ , as in Fig. 1. Events are labelled as "elastic" if the energy deposited in the calorimeter is less than  $\approx 5$  GeV. Conventionally, elastic  $\psi$  and unbound  $c\bar{c}$  muoproduction are compared to predictions of the leading-order photon-gluon fusion ( $\gamma$ GF) subprocess diagrammed in Table V. Shown there as well are the next-to-leading order subprocesses,  $\gamma q \rightarrow (c\bar{c})g$  and  $\gamma q \rightarrow (c\bar{c})q$ , and a partial list of recent calculations<sup>18-27</sup> using these diagrams. The  $\gamma$ GF process obviously fails to conserve color. If the  $c\bar{c}$  pair is bound into a  $\psi$ , C-parity also is not conserved. This is fixed up by assuming that additional, soft gluon exchange(s) take place but do not appreciably affect the kinematics. Thus, the extent to which the target state is excited, i.e. the extent to which the process is inelastic, is precisely specified neither by the muon data nor by the lowest-order calculation.

Input parameters to  $\gamma$ GF are  $\alpha_s$ , evaluated near  $m_{c\bar{c}}^2 \approx 10(\text{GeV}/c)^2$ ; the charmed quark mass  $m_c$ , typically  $1.5 \text{ GeV}/c^2$ ; and the distribution  $G(x)$  (typically,  $3(1-x)^5/x$  at  $Q^2 \approx m_{c\bar{c}}^2$ ) in momentum fraction  $x$  (or  $\eta$ ) of massless gluons. With these approximations the  $c\bar{c}$  pair is produced at  $t \equiv t_{\min}$ , with an invariant-mass distribution peaking between  $4.5$  and  $5 \text{ GeV}/c^2$  at typical energies. According to the "semilocal duality" ansatz, predictions apply to bound (unbound)  $c\bar{c}$  production when  $m_{c\bar{c}}$  is less than (greater than)  $2m_p$ ;  $\psi$  production is represented by an unspecified fixed fraction of bound  $c\bar{c}$  production. Predicted are the total cross section for  $c\bar{c}$  muoproduction, and, with semilocal duality, the  $Q^2$  and  $\nu$  dependence for elastic  $\psi$  and open  $c\bar{c}$  final states. In the case of  $\psi$  muoproduction, the behavior in  $t$ , in elasticity  $z = E(\psi)/E(\gamma)$ , and in  $\psi$  polarization also can be measured with useful resolution. Because of the approximations described above,  $\gamma$ GF makes no clear prediction in these areas.

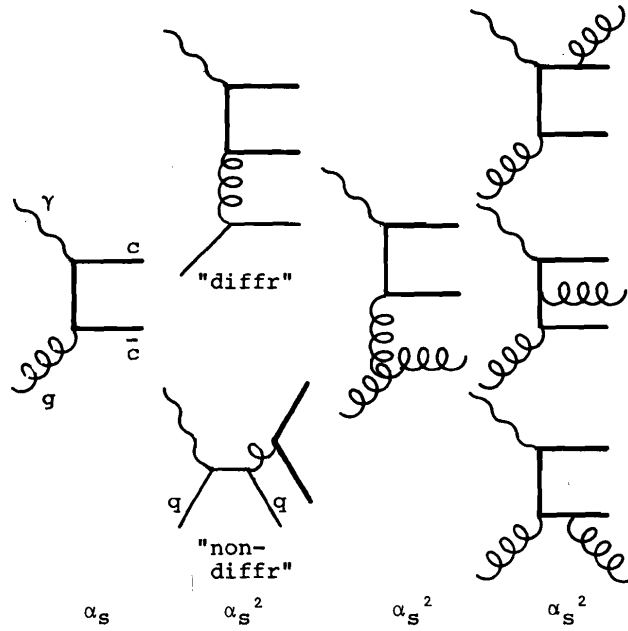
II.2 Angular Distributions

The BFP experiment has obtained distributions<sup>8</sup> in three angular variables pertinent to elastic  $\psi$  production. These are illustrated in Fig. 5. The first angle is  $\phi_{21}$ , the difference between azimuths of the  $\gamma\gamma N \rightarrow \psi N$  diffraction plane and the muon scattering plane, using the  $\gamma\gamma$  direction as an axis. A crude analysis of its distribution (Fig. 6) reveals no obvious structure, in contrast to the  $\gamma$ GF prediction<sup>20</sup> of measurable [10-15% at  $p_{\perp}^2 = 0.5(\text{GeV}/c)^2$ ]  $\cos \phi_{21}$  asymmetry arising from gluon intrinsic transverse momenta. Also indicated in Fig. 5 is  $\phi_{32}$ , the difference between azimuths of the  $\psi \rightarrow \mu^+\mu^-$  decay plane and the aforementioned diffraction plane, using the  $\psi$  direction as an axis. The second angle which we shall consider is  $\Delta\phi$ , the difference between  $\phi_{32}$  and  $\phi_{21}$ . The third angle  $\Theta$  is the polar angle of the  $\psi \rightarrow \mu^+\mu^-$  decay, defined in a  $\psi$  rest frame boosted along the  $\psi$  direction as seen in the  $\gamma\gamma N$  cms (i.e. in the s-channel helicity frame).

Assuming s-channel helicity conservation (SCHC) and natural parity exchange,

Table V. Recent calculations of  $c\bar{c}$  photo- and electroproduction via gluons.

| Diagram name or remark<br>(crossed diagrams omitted) | $\gamma$ GF<br>(elastic<br>or diffr) | Recoil<br>quark | 3 gluon | $C^-$ color<br>singlet $c\bar{c}$<br>allowed |
|--|--------------------------------------|-----------------|---------|--|
|--|--------------------------------------|-----------------|---------|--|



Order

Assumptions:  $c\bar{c} \rightarrow \psi$

"Semilocal duality"

Can use normalized  $\psi$  wavefunction

Authors                      Ref    States

|                         |    |                                 |         |
|-------------------------|----|---------------------------------|---------|
| Weiler                  | 18 | $\gamma_V \rightarrow c\bar{c}$ | ✓       |
| Barger, Keung, Phillips | 19 | $\gamma_V \rightarrow c\bar{c}$ | ✓       |
| Leveille & Weiler       | 20 | $\gamma_V \rightarrow c\bar{c}$ | ✓       |
| Leveille & Weiler       | 21 | $\gamma_V \rightarrow c\bar{c}$ |         |
| Duke & Owens            | 22 | $\gamma \rightarrow c\bar{c}$   | ✓       |
| Duke & Owens            | 23 | $\gamma_V \rightarrow c\bar{c}$ | ✓       |
| Duke & Owens            | 24 | $\gamma \rightarrow c\bar{c}$   | ✓ and x |
| Tajima & Watanabe       | 25 | $\gamma \rightarrow c\bar{c}$   | ✓       |
| Berger & Jones          | 26 | $\gamma \rightarrow \psi$       | ✓       |
| Keung                   | 27 | $\gamma_V \rightarrow \psi$     | ✓       |

"diffr"  
only

✓                      ✓                      ✓  
✓                      ✓                      ✓  
✓ and x              ✓ and x              ✓  
✓                      ✓                      ✓

the expected distribution in  $\theta$  and  $\Delta\phi$  is<sup>10</sup>

$$W(\eta, R) = [3/16\pi(1+\epsilon R)] \{1 + \cos^2\theta + 2\epsilon R \sin^2\theta - \eta \epsilon \sin^2\theta \cos 2\Delta\phi\}, \quad (1)$$

where  $\epsilon \approx 0.8$  is the ratio of longitudinal to transverse photon flux,  $R$  is the longitudinal/transverse  $\psi$  production ratio  $\sigma_L/\sigma_T$ , and  $\eta$  is a factor nominally equal to unity, introduced to monitor the size of the fit  $\cos 2\Delta\phi$  term. Additional terms which average to zero or are orthogonal to  $\cos 2\Delta\phi$  over the interval  $-\pi < \Delta\phi < \pi$  are omitted, in anticipation of the use of twice-folded  $\phi_F \equiv (\cos^{-1} |\cos 2\phi|)/2$  in Fig. 7. The obvious feature in that Figure is the strong  $\cos 2\Delta\phi$  dependence of the data, unpredicted by any  $\gamma$ GF calculation. If binned in  $|\cos\theta|$ ,  $\phi_F$ , and  $Q^2$ , and fit to  $W(\eta, R) \times P(\Lambda)$ , where  $P(\Lambda) = (1 + Q^2/\Lambda^2)^{-2}$ , the best fit  $\eta \approx 1$  saturates the SCHC expectation (Table VI).

In brief summary, the  $\gamma$ GF model predicts structure in  $\phi_{21}$  which is not obvious in the data, and is prevented by its own approximate nature from predicting sizable observed structure in  $\Delta\phi$ .

### II.3 $Q^2$ and $\nu$ Dependence

The first measurements<sup>6,7</sup> of elastic  $\psi$  muoproduction fit its  $Q^2$ -dependence to a propagator  $P(\Lambda)$ , obtaining  $\Lambda = 2.7 \pm 0.5$  and  $\Lambda = 2.4 \pm 0.3$  GeV/c<sup>2</sup>, respectively. These simple fits made no allowance for any additional  $Q^2$ -dependence in the decay angular distribution, for example the dependence of  $R = \sigma_L/\sigma_T$  on  $Q^2$  near  $Q^2 = 0$  (Eq. 1). Table VI presents the final results<sup>8</sup> of the BFP group's fits simultaneously to  $\Lambda$ ,  $R$ , and  $\eta$ , with and without a screening factor  $S(x') = [1 - 0.33 \exp(-28x')]^{0.76}$ . For any case allowed by the data,  $\Lambda$  is between 1.9 and 2.6 GeV/c<sup>2</sup>, with the nominal value  $2.2 \pm 0.2$ . This is at least 4 standard deviations from  $\psi$  dominance ( $\Lambda = 3.1$ ). In Fig. 8 the tendency of the BFP data to lie below both the  $\psi$  dominance and  $\gamma$ GF predictions is readily apparent.

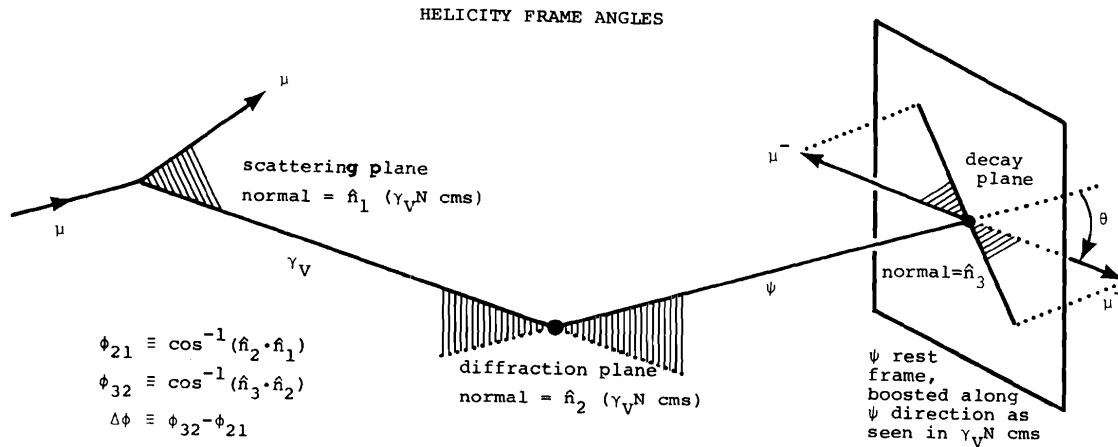


Fig. 5. Illustration of helicity frame angles.  $\phi_{21}$  is sensitive to the angular correlation between  $\gamma_V$  polarization and  $\gamma_V N \rightarrow \psi N$  diffraction;  $\Delta\phi$  in addition is sensitive to the  $\psi$  polarization.

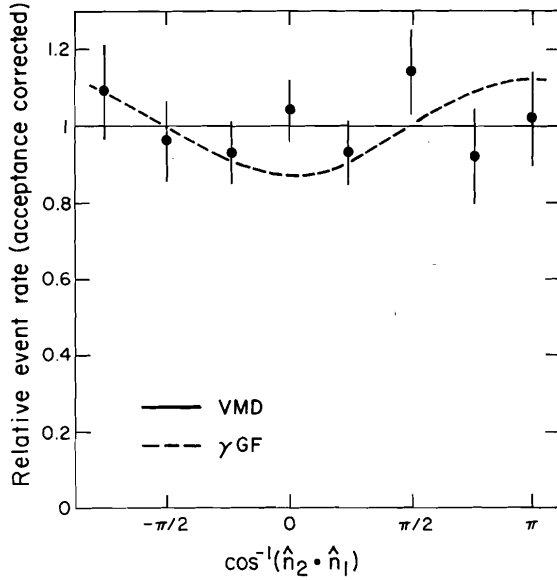


Fig. 6. Distribution of BFP elastic + inelastic  $\psi$  data in  $\phi_{21} = \cos^{-1}(\hat{n}_2 \cdot \hat{n}_1)$  [Fig. 5]. The analysis is much more crude than in Ref. 10: subtraction of background under the  $\psi$  peak and  $\phi_{21}$  resolution smearing are neglected, and the acceptance is only crudely corrected. Nevertheless, the absence of obvious  $\cos \phi_{21}$  structure, when compared to the  $\gamma$ GF prediction (Ref. 20), may be significant.

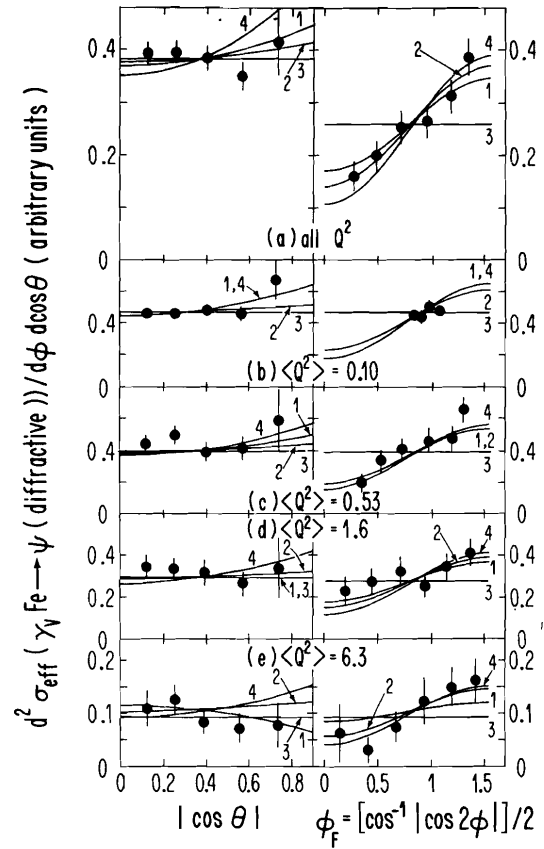


Fig. 7. Angular dependence of the effective cross section for the reaction  $\gamma_V Fe \rightarrow \psi X$  (energy of  $X < 4.5$  GeV). BFP data and statistical errors are presented vs  $|\cos \theta|$  (left column) and  $\phi_F$  (right column), where  $\phi_F$  is  $\Delta\phi$  folded into one quadrant;  $\theta$  and  $\Delta\phi$  are defined in Fig. 5. All data ( $\langle Q^2 \rangle = 0.71$ ) are shown in (a); (b)-(e) divide the data into four  $Q^2$  regions. Numbered solid lines exhibit the results of fits 1-4 in Table VI. Fits 1, 2, and 4 are to the SCHC formula with  $\sigma_L/\sigma_T = \xi^2 Q^2/m_\psi^2$ , const, and 0, respectively; fit 3 corresponds to the production of unpolarized  $\psi$ 's.

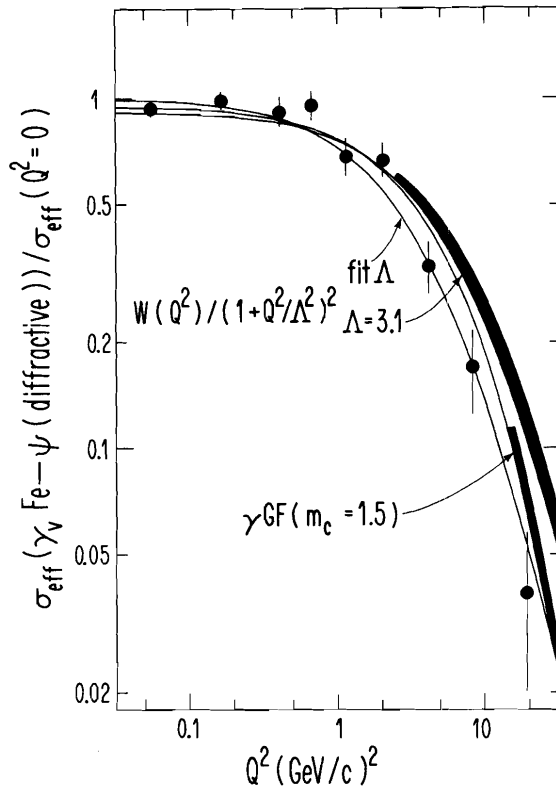


Fig. 8.  $Q^2$  dependence (BFP data) of the effective cross section for the reaction  $\gamma_V \text{Fe} \rightarrow \psi X$  (energy of  $X < 4.5$  GeV). Statistical errors are shown. The data are fitted to  $(1+Q^2/\Lambda^2)^{-2}$  multiplied by the function  $W(\eta, R)$  shown in Table VI. The best fits with free  $\Lambda$  (Table VI, fit 1) and fixed  $\Lambda=3.1$  (Table VI, fit 5) are shown. The data are normalized so that fit 1 is unity at  $Q^2=0$ . Also exhibited is the  $\gamma$ GF prediction (Table VI, fit 7). At high  $Q^2$ , fits 1 and 7 are displayed as a solid band, with the upper (lower) edge including (omitting) the screening factor  $S(x')$ .

TABLE VI. BFP fits to the  $Q^2$ ,  $\phi$ , and  $\theta$  dependence of the effective cross section  $\sigma_{\text{eff}}$  for the reaction  $\gamma_V \text{Fe} \rightarrow \psi X$  (energy of  $X < 4.5$  GeV). The angular function  $W(\eta, R)$ , propagator  $P(\Lambda)$ , and nuclear screening factor  $S(x')$  are defined in the text. Each of seven fits (numbered in the first column) is performed both with  $S(x')$  included (multiplied "in") and ignored ("out") in the function fitted. Errors on the fit parameters  $\Lambda$ ,  $\eta$ , and  $\xi^2$  (fits 1 or 6) or  $R$  (fit 2) are statistical. Fit 6 is the same as fit 1 except that  $W$  is multiplied by  $(1+\epsilon R)$ ;  $\Lambda$  then parameterizes the  $Q^2$  dependence of  $\sigma_T$  rather than  $\sigma_{\text{eff}}$ . Fit 7 compares the data integrated over  $\phi$  and  $\cos\theta$  with the  $Q^2$  dependence predicted by  $\gamma$ GF.

| Fit No. | Function   | $S(x')$ | $\chi^2/\text{DF}$ | $\Lambda(\text{GeV}/c^2)$         | $\eta$                 | $\xi^2$ or $R$        |
|---------|--|---------|--------------------|-----------------------------------|------------------------|-----------------------|
| 1       | $W(\eta, R) \times P(\Lambda)$<br>$R = (\xi Q/m_\psi)^2$ | in      | 45.4/56            | $2.03^{+0.18}_{-0.12}$            | $1.02^{+0.28}_{-0.23}$ | $3.3^{+4.9}_{-3.0}$   |
|         |  | out     | 45.5/56            | $2.18^{+0.18}_{-0.13}$            | $1.04^{+0.28}_{-0.23}$ | $4.0^{+4.8}_{-3.4}$   |
| 2       | $W(\eta, R) \times P(\Lambda)$<br>$R = \text{constant}$  | in      | 42.0/56            | $2.24 \pm 0.13$                   | $1.09^{+0.31}_{-0.24}$ | $.55^{+0.26}_{-0.18}$ |
|         |  | out     | 42.4/56            | $2.43 \pm 0.15$                   | $1.10^{+0.31}_{-0.24}$ | $.37^{+0.27}_{-0.22}$ |
| 3       | $1 \times P(\Lambda)$                                    | in      | 73.3/58            | $2.06 \pm 0.11$                   |                        |                       |
|         |  | out     | 73.3/58            | $2.22 \pm 0.13$                   |                        |                       |
| 4       | $W(1, 0) \times P(\Lambda)$                              | in      | 48.6/58            | $2.21 \pm 0.12$                   | $\approx 1$            | $\approx 0$           |
|         |  | out     | 49.3/58            | $2.40 \pm 0.14$                   |                        |                       |
| 5       | $W(\eta, 0) \times P(m_\psi)$                            | in      | 89.1/58            | $\approx 3.1$                     | $0.96 \pm 0.13$        | $\approx 0$           |
|         |  | out     | 68.5/58            |                                   | $0.93 \pm 0.14$        |                       |
| 6       | $(1+\epsilon R) \times \text{Fit 1}$                     | in      | 47.0/56            | $2.08 \pm 0.24$                   | $0.86 \pm 0.17$        | $.24^{+0.61}_{-0.39}$ |
|         |  | out     | 47.6/56            | $2.20 \pm 0.29$                   | $0.87 \pm 0.17$        | $.34^{+0.75}_{-0.43}$ |
| 7       | $\gamma$ GF -- $Q^2$<br>projection                       | in      | 32.1/8             |                                   |                        |                       |
|         |  | out     | 14.6/8             | $m_c \approx 1.5 \text{ GeV}/c^2$ |                        |                       |

Detailed comparison of the BFP data<sup>10</sup> to  $\gamma$ GF predictions is best made after integrating over  $\theta$  and  $\Delta\phi$ , where  $\gamma$ GF makes no predictions, and binning the events in a  $Q^2, \nu$  grid. Roughly speaking, in that model the  $Q^2$ -dependence is sensitive to the parameter  $m_C$ ; the  $\nu$ -dependence is sensitive both to the gluon momentum distribution, i.e. to  $n$  in  $G(x) \propto (1-x)^n/x$ , and to  $m_C$  through the relation  $x = (Q^2 + m_C^2)/2m\nu$ . Suppressing for a moment the  $Q^2$ -dependence, Fig. 9(a) shows the  $\nu$ -dependence of BFP data extrapolated to  $Q^2=0$ , together with  $\psi$  photoproduction data from the SLAC-Wisconsin experiment<sup>28</sup>. With  $m_C=1.5$  GeV/c<sup>2</sup>, the exponent  $n$  characterizing the gluon distribution is  $5.3 \pm 0.4$ , in agreement with the "counting-rule" value 5, and with earlier fits<sup>18,19</sup> to earlier data<sup>6,7</sup>. When the BFP data are binned in the  $Q^2, \nu$  grid (Fig. 9(b)), the steep  $Q^2$ -dependence fixes  $m_C$  at  $1.10 \pm 0.08$  GeV/c<sup>2</sup>; to fit the  $\nu$ -dependence with this smaller  $m_C$ ,  $n$  is forced up to  $9.2 \pm 1.2$ ! The  $\psi$  muoproduction cross section predicted by  $\gamma$ GF and "semilocal duality", already too high, rises further by a factor of 8.4 when these new parameters are used.

Evidently, while accounting sensibly for the  $\nu$ -dependence of the data extrapolated to  $Q^2=0$ , the  $\gamma$ GF model does not simultaneously explain the steep  $Q^2$ -dependence of  $\psi$  muoproduction and its observed cross section.

#### II.4 Bound Charm Cross Sections

Measured and predicted cross sections for various charm muoproduction and photoproduction processes are listed in Table VII. Elastic  $\psi$  muoproduction has a measured cross section of  $0.36 \pm 0.01 \pm 0.07$  nb (BFP data). The "standard"  $\gamma$ GF calculation ( $m_C=1.5$ ,  $n=5$ ) together with "semilocal duality" predict 2.8 nb for all charmonia, when  $\alpha_S=0.41$  ( $\Lambda=0.5$  GeV/c<sup>2</sup>). If  $\alpha_S=0.22$  ( $\Lambda=0.1$ ), the prediction is 1.5 nb. Where are the other 2.4 or 1.1 nb?

The contribution from muoproduced or photoproduced charmonia other than the  $1^-$  states has not been measured. The  $\psi'$  contribution may be inferred from new Fermilab-Illinois photoproduction data<sup>9</sup>. Shown in Fig. 10 is the  $\psi\pi^+\pi^-$  mass spectrum of four-prong events which contain dileptons near the  $\psi$  mass. A convincing  $\psi'$  peak is observed. At 160 GeV, the diffractive  $\psi'$  photoproduction cross section is  $6 \pm 1.5$  nb, or 19 $\pm$ 6% of the  $\psi$  cross section. Therefore,  $\psi'$  muoproduction accounts for less than 0.1 of the missing 2.4 or 1.1 nb. It is unlikely that production of other charmonia, with quantum numbers different from those of the photon, can make up the difference. Probably the combination of photon-gluon fusion and semilocal duality overestimates the bound charm cross section by a factor 2-5.

I shall defer a critical summary of the status of lowest-order  $\gamma$ GF to the next section, after relevant open-charm data are discussed.

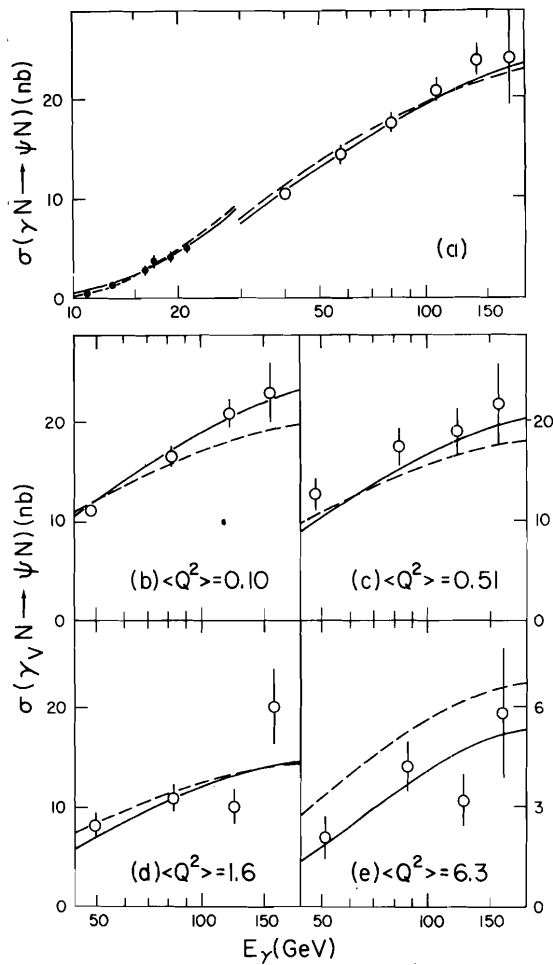


Fig. 9. (a) Effective cross section  $\sigma_{\text{eff}}$  vs.  $E_\gamma$  for the diffractive process  $\gamma N \rightarrow \psi N$ . Superimposed are  $\gamma$ GF fits with  $m_c$  variable (solid curve) and fixed to  $1.5 \text{ GeV}/c^2$  (dashed curve); for the latter fit the exponent of  $(1-\eta)$  is  $5.3 \pm 0.4$ . The break in the curve arises from allowing for a relative normalization difference, consistent with quoted scale errors, between the SLAC-Wisconsin photoproduction data (solid points) and BFP data extrapolated to  $Q^2=0$  (open points). (b)-(e)  $\sigma_{\text{eff}}$  vs.  $E_\gamma$  for four  $Q^2$  regions. The solid curves correspond to  $m_c = 1.10 \pm 0.08 \text{ GeV}/c^2$ , with the exponent of  $(1-\eta)$  equal to  $9.2 \pm 1.2$ .

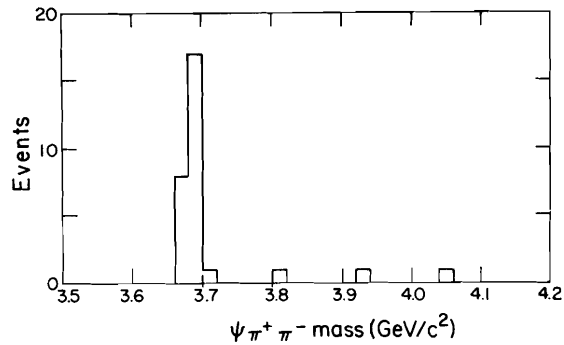


Fig. 10. Invariant mass of  $\psi \pi^+ \pi^-$  for Fermilab-Illinois wideband photoproduction data using  $\text{H}_2$  and  $\text{D}_2$  targets. The  $\psi$ 's are identified by a cut on the  $\mu^+ \mu^-$  or  $e^+ e^-$  mass. At  $160 \text{ GeV}$ ,  $\sigma(\gamma N \rightarrow \psi' X)$  (diffractive) =  $6 \pm 1.5 \text{ nb}$ , corresponding to  $\sigma(\psi')/\sigma(\psi) = 0.19 \pm 0.06$ .

Table VII. Charm electro- and photoproduction cross sections.

| Process  | Group | Ref | Cross section<br>(nb)    | Energy<br>(GeV) | Prediction<br>(nb)                     |
|--|-------|-----|--------------------------|-----------------|--|
| $\mu N \rightarrow \psi N$ (elastic)                       | BFP   | 10  | $0.36 \pm 0.01 \pm 0.07$ | 209             | $2.8 (\times \text{duality factor})^a$ |
| $\mu N \rightarrow \psi X$ (inelastic)                     | BFP   | 10  |                          |                 |  |
| $z > 0.7$  |       |     | $0.14 \pm 0.01 \pm 0.02$ | 209             |  |
| $z < 0.7$  |       |     | $0.14 \pm 0.01 \pm 0.03$ | 209             |  |
| all $z$  |       |     | $0.28 \pm 0.03 \pm 0.05$ | 209             |  |
| $\mu N \rightarrow \psi X$ (elastic<br>+ inelastic)        | BFP   | 10  | $0.64 \pm 0.03 \pm 0.10$ | 209             |  |
| $\mu N \rightarrow c\bar{c}X$ (unbound)                    | BFP   | 13  | $6.9^{+1.9}_{-1.4}$      | 209             | $5.0^a$                                |
| $\gamma N \rightarrow \psi N$ (elastic)                    | BFP   | 10  | $10.3 \pm 0.8$           | 40              | 20%<br>scale<br>error                  |
|  |       |     | $14.3 \pm 0.9$           | 58              |  |
|  |       |     | $17.5 \pm 0.9$           | 80              |  |
|  |       |     | $20.7 \pm 1.2$           | 108             |  |
|  |       |     | $23.8 \pm 1.6$           | 140             |  |
|  |       |     | $24.0 \pm 5.0$           | 173             |  |
| $\gamma N \rightarrow \psi X$ (inelastic)<br>( $z < 0.9$ ) | BFP   | 10  | $7.6 \pm 1.3$            | 42              | 20%<br>scale<br>error                  |
|  |       |     | $11.1 \pm 1.0$           | 58              |  |
|  |       |     | $12.7 \pm 1.0$           | 81              |  |
|  |       |     | $16.8 \pm 1.3$           | 111             |  |
|  |       |     | $22.1 \pm 1.8$           | 144             |  |
|  |       |     | $26.4 \pm 3.5$           | 178             | $3.3^b$                                |
| $\gamma N \rightarrow c\bar{c}X$ (unbound)                 | BFP   | 13  | $560^{+200}_{-120}$      | 100             |  |
|  |       |     | $750^{+180}_{-130}$      | 178             |  |

<sup>a</sup> $\gamma_{GF}$  with  $\eta G(\eta) = 3(1-\eta)^5$ ,  $\alpha_S = 1.5/\ln(4m_{c\bar{c}}^2)$ ,  $m_c = 1.5 \text{ GeV}/c^2$ .

<sup>b</sup> $\gamma_{G \rightarrow \psi G}$  result (Ref 26) multiplied by 0.7 (calculated fraction with  $z < 0.9$ ).

## III. OPEN-CHARM MUOPRODUCTION

III.1 Background

The signature for open-charm production in the muon data<sup>11-16</sup> is provided by one<sup>11,13-16</sup> or two<sup>12</sup> decay muons from the pair-produced charmed states. In the latter case, discrimination between hadronic and electromagnetic showers in the calorimeter together with missing-energy criteria are used to discriminate against inelastic QED-induced trimuons. In the former case, depending on cuts in  $\nu$ ,  $Q^2$ , and  $p_{\perp}$  (the produced muon momentum  $\perp$  to the  $\gamma_V$  direction), the background from  $\pi$  and K decay amounts to 10-20%. In the EMC<sup>11-12,16</sup> and BFP<sup>13-15</sup> analyses, this calculated background is absolutely normalized and subtracted from the charm signal; BFP assigns<sup>15</sup> a 50% systematic error to this procedure.

In both experiments a major limitation on the acceptance is imposed by a  $\approx 15$  GeV lower bound on the detectable muon momentum. This limitation is far more severe than in  $\psi$  production: the exchanged photon energy is divided among a minimum of six charm decay products, in addition to any light mesons produced together with the charmed states. Comparison with charm-production mechanisms depends strongly on the model used for charmed quark fragmentation and decay. In their 1980 publications EMC<sup>11,12</sup> quoted "cut cross sections" based on 497 dimuons and 120 trimuons observed within a restricted kinematic region. Cross sections based on the 20 072-event BFP dimuon sample<sup>13,14</sup> were corrected to uncut values using a range of charm fragmentation assumptions allowed by the same data (Table VII). Newly available preliminary EMC results<sup>16</sup>, based on 3150 dimuons and 117 trimuons, also have been corrected for cuts, using particular fragmentation hypotheses; it is convenient now to compare results from the two experiments.

III.2 Charm Structure Function

The charm structure function  $F_2(c\bar{c})$  is defined by

$$d^2\sigma(\mu N + \mu c\bar{c}X)/dQ^2 d\nu = (4\pi\alpha^2/Q^4 \nu) (1-y+y^2/2) F_2(c\bar{c}). \quad (2)$$

$F_2(c\bar{c})$  plays the same role in charm production as would  $F_2$  in inclusive scattering if absorption of longitudinally polarized photons were negligible. In the notation of Ellis<sup>29</sup>

$$F_2^{\mu N}(x_{BJ}) = x_{BJ} \left[ \frac{5}{18}(u+\bar{u}) + \frac{5}{18}(d+\bar{d}) + \frac{1}{9}(s+\bar{s}) + \frac{4}{9}(c+\bar{c}) + \dots \right] \quad (3)$$

Equations (2) and (3) identify  $F_2(c\bar{c}) \approx 4x_{BJ}(c+\bar{c})/9$ .

The data are reasonably well described<sup>11-15</sup> by the lowest-order  $\gamma$ GF calculation. In that picture, the modest calculated values of  $m_{c\bar{c}}$  require the exchanged photon energy to be more or less equally shared by both charmed quarks. For representative parameterizations of charmed quark fragmentation, one obtains a much softer produced muon energy spectrum than in a "struck charmed quark" model in which one charmed quark inherits most of the exchanged energy. For that reason, the experimental acceptance calculated in the  $\gamma$ GF model is smaller than in the struck quark picture; however, twice as many fast charmed quarks are available for decay into muons. Therefore it is risky and possibly misleading to

use a  $\gamma$ GF model calculation to unfold acceptance and branching ratio effects in determining  $c(x_{BJ}) + \bar{c}(x_{BJ}) = 9F_2(c\bar{c})/4x_{BJ}$ , if the objective is to determine the "charmed sea" appropriate to a "struck quark" picture of charm muoproduction. Instead it is better to use the struck quark model to generate predictions for comparison to experimental distributions or to "cut cross sections". The latter method was used by the EMC group<sup>11</sup> to rule out the struck quark process as a major contributing factor. A similar conclusion follows from their observation<sup>12</sup> of fast muons from the decay of both charmed quarks at levels consistent with  $\gamma$ GF.

### III.3 Comparison of the Data

Figure 11 compares the charm structure function published<sup>14</sup> by BFP to new results<sup>16</sup> from EMC. For each value of the indicated parameter, (open) BFP and (closed) EMC points are represented by the same symbol shape; absolute normalizations have been adjusted to minimize discrepancies. At fixed  $x_{BJ}$  the EMC data extend to lower  $Q^2$ ; this is because the BFP data are cut at  $\nu > 75$  GeV to minimize systematic uncertainties (section III.6). The agreement is very good, save for the points at  $x_{BJ} = 0.042$ ,  $Q^2 \approx 13$  (GeV/c)<sup>2</sup>, which differ by  $\approx 40\%$ . These are split by the model curve, which uses the  $Q^2$ -developed Glück-Hoffmann-Reya glue<sup>30</sup>; undeveloped "counting-rule" glue gives as acceptable a fit<sup>16</sup>. As expected from charmed-quark mass effects, the charm structure function shown in Fig. 11 is strongly scale-noninvariant. Diffractive charm production contributes<sup>14</sup>  $\approx 30\%$  of the inclusive scale-noninvariance  $\partial F_2^{\mu N} / \partial \ln Q^2$  in a region centered at  $\langle Q^2 \rangle \approx 5$  (GeV/c)<sup>2</sup>,  $\langle x_{BJ} \rangle \approx 0.025$ .

### III.4 Open-Charm Cross Sections

The available cross-section measurement<sup>13</sup> for charm muoproduction is reproduced in Table VII, along with the corresponding effective photoproduction cross sections  $\sigma_{\text{eff}}$ . The latter were obtained<sup>13</sup> by extrapolating  $\sigma_{\text{eff}}(Q^2)$  to  $Q^2 = 0$  according to  $(1 + Q^2/\Lambda^2)^{-2}$ , with best-fit propagator masses  $\Lambda = 2.9 \pm 0.2$  ( $3.3 \pm 0.2$ ) GeV/c<sup>2</sup>, at  $\nu = 100$  (178) GeV.

Since the "semilocal duality" ansatz causes  $\gamma$ GF to overestimate the observed bound-charm muoproduction cross section (section II.4), it is interesting to test the  $\gamma$ GF cross-section predictions independently of semilocal duality. At 209 GeV, the cross section for muoproduction of (bound + unbound) charm is predicted by  $\gamma$ GF to be  $2.8 + 5.0 = 7.8$  nb ( $1.5 + 2.7 = 4.2$  nb) with  $\alpha_s = 0.41$  (0.22), i.e.  $\Lambda = 0.5$  (0.1) GeV/c. The observed elastic  $\psi$  cross section<sup>10</sup> is 0.36 nb; elastic  $\psi'$  production contributes 0.07 nb. Open  $c\bar{c}$  muoproduction accounts for  $6.9_{-1.4}^{+1.9}$  nb. Inelastic  $\psi$  production contributes 0.28 nb; it is not clear (section II.1) whether this and other inelastic bound charm production should be included in the total to be compared to  $\gamma$ GF. Ascribing (0-1.8) nb to the appropriate sum of inelastic  $\psi$ , inelastic  $\psi'$ , and non- $1^-$  charmonium production, the experimental grand total is 6-11 nb. This is better agreement with  $\gamma$ GF than might have been expected, given the approximations. The  $\gamma$ GF prediction is highly sensitive to  $m_c$ , which therefore may be regarded as forced to  $\approx 1.5$  GeV/c<sup>2</sup> by this agreement.

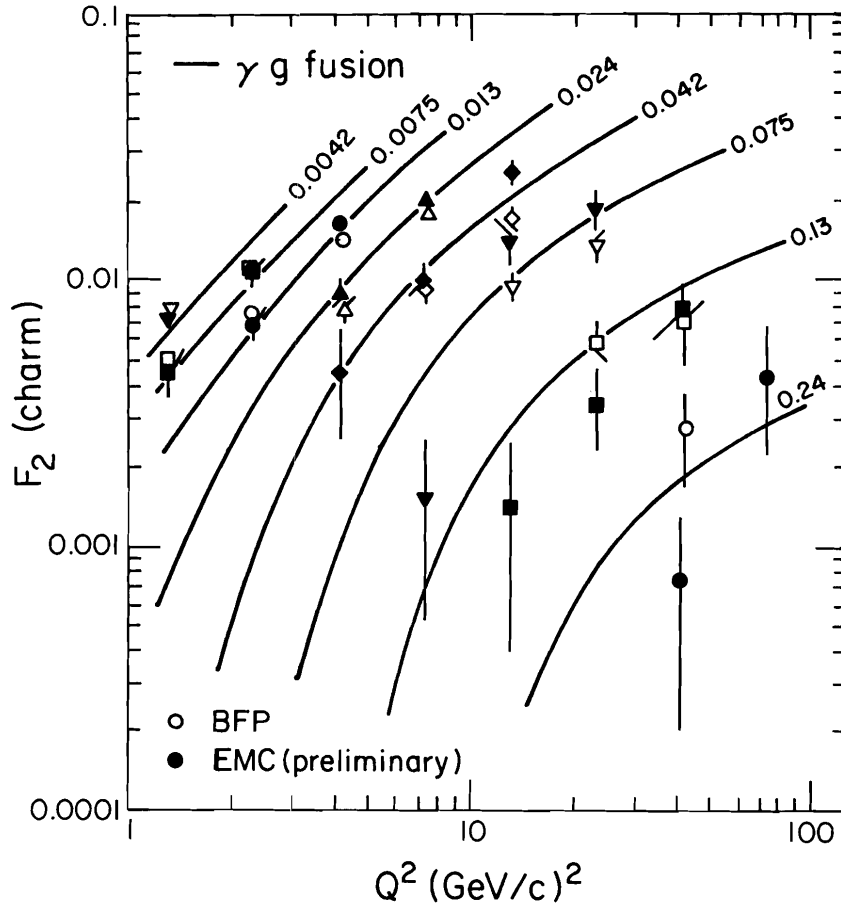


Fig. 11. Charm structure function  $Q^2\nu/[4\pi\alpha^2(1-y+y^2/2)]d^2\sigma(c\bar{c})/dQ^2d\nu$  vs.  $Q^2$  with  $x_{BJ}=Q^2/2m\nu$  as the indicated fixed parameter. Open points are published BFP data (Ref. 14) based on 20 072 events; closed points are privately communicated EMC data (Ref. 16) based on 3150 events. Errors are statistical. The quoted BFP (EMC) scale error is  $\pm 20\%$  ( $\pm 40\%$ ); BFP points have been multiplied by 0.9 to facilitate the comparison. The curves, arbitrarily normalized to the EMC data, are a  $\gamma$ GF calculation based on the gluon distribution  $\eta G(\eta)[Q^2=4] = 0.93 \times (1+8.56\eta + 56.3\eta^2)(1-\eta)^6$ , developed using an effective  $Q^2$  equal to  $Q^2+m^2_{c\bar{c}}$ . As good a fit is achieved with the undeveloped  $(1-\eta)^5$  "counting-rule" glue.

### III.5 Data vs. Photon-Gluon Fusion - A Summary

The phenomenological successes of  $\gamma$ GF are the following:

- (1) Factor-of-two prediction of the charm muoproduction cross section (however, "semilocal duality" probably overestimates the ratio of bound to unbound charm).
- (2) Good agreement with the  $\nu$ -dependence of bound and unbound charm production, using  $\approx 3(1-x)^5/x$  glue at effective  $Q^2 \approx 10$  (GeV/c)<sup>2</sup>.
- (3) Agreement in  $Q^2$ -dependence which is satisfactory for open charm, but only fair (data too steep) for bound charm muoproduction. The "semilocal duality" boundary  $m_{c\bar{c}} = 2m_D$  between bound and open charm complicates fitting  $m_c$  to these data. Overall, the agreement between data and  $\gamma$ GF in  $Q^2$  is as successful as for Vector Dominance.

Up to this point, the primary phenomenological shortcoming of  $\gamma$ GF is its inability to account for the angular dependences observed for  $\psi$  muoproduction (section II.2).

It is useful here to recall two philosophical shortcomings of photon-gluon fusion. In section II.1 I mentioned the neglect of effects associated with necessary additional soft gluon exchange. A related worry is  $\gamma$ GF's use of a parton-model parameterization of the gluon distribution to describe a process which does not guarantee appreciable four-momentum transfer to the target. In elastic  $\psi$  muoproduction,  $Q^2$  can be  $> 10$  (GeV/c)<sup>2</sup> and  $W^2$  can be  $> 200$  (GeV/c)<sup>2</sup> while  $-t$  is small enough to allow the target nucleon or even the target nucleus not to become excited. Likewise in the open charm experiments, the calorimeter does not distinguish between energy deposited by target excitation, if any, and energy deposited by hadrons associated with D or D\* decay. For example, the data sample can include dissociation of exchanged photons into DD\*, when diffracted by nucleons or coherently by Fe nuclei. To believe  $\gamma$ GF we must understand how it is that nucleon constituents may be measured with so gentle a probe.

### III.6 Fitting the Gluon Distribution Using Open-Charmed Muoproduction

If uncertainties about the validity of the  $\gamma$ GF model can be overcome, the high statistics available to either open-charm experiment in principle should lead to precise determination of the gluon distribution in the nucleon. Roughly speaking,  $G(x)$  is determined by the  $\nu$  distribution of the data, if  $m_c$  is fixed (for example) by absolute cross section measurement. The  $Q^2$  distribution of the data is sensitive to  $m_{c\bar{c}}$ . This would give another constraint on  $m_c$ , except for the lower bound  $m_{c\bar{c}} > 2m_D$  enforced by "semilocal duality". In the presence of this bound, the  $\gamma$ GF prediction for the  $Q^2$  shape instead is influenced primarily by the argument of  $\alpha_s$ :  $\alpha_s(m_{c\bar{c}}^2 + Q^2)$  fits better<sup>31</sup> than  $\alpha_s(m_{c\bar{c}}^2)$  if  $\Lambda = 0.5$  GeV/c.

Unfortunately, the process either of correcting the  $\nu$ -dependence of the data up to an uncut cross section, or of correcting any gluon model down to a cut cross section, is highly sensitive to the assumed charmed-quark fragmentation function (section III.1). The fragmentation variable  $z = E_D/E_D(\max)$  may be applied<sup>31</sup> in the  $c\bar{c}$  rest frame assuming diffractive  $c\bar{c}$  production (as in the BFP analysis<sup>15</sup>) or in the target rest frame assuming more central  $c\bar{c}$  production (as in the EMC analysis<sup>16</sup>). In either case the fragmentation function is varied within limits

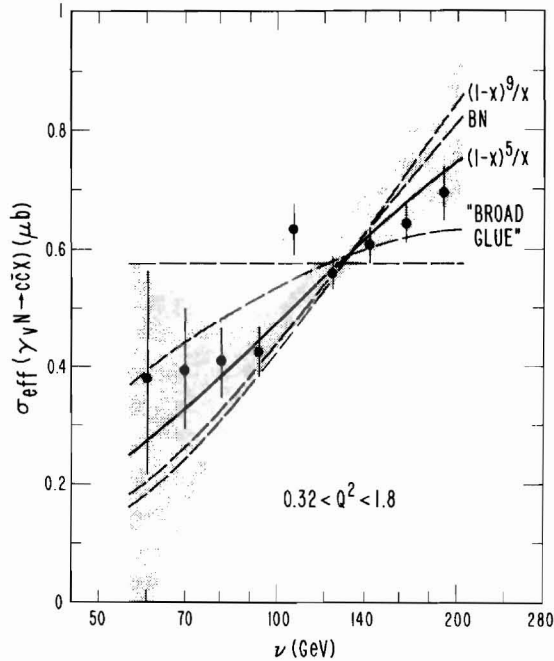


Fig. 12. Energy dependence (BFP data) of the effective cross section  $\sigma_{\text{eff}}$  for diffractive charm photoproduction. For  $0.32 < Q^2 < 1.8$  ( $\text{GeV}/c^2$ ),  $\sigma_{\text{eff}}$  varies with  $Q^2$  by  $\lesssim 20\%$ . Errors are statistical. The solid curve exhibits the  $\nu$  dependence of the photon-gluon fusion model with the "counting-rule" gluon  $x$  distribution  $3(1-x)^5/x$ , and represents the data with 13% confidence. Other gluon-distribution choices  $(1-x)^9/x$ , and "broad glue"  $(1-x)^5$  ( $13.5+1.07/x$ ) are indicated by dashed lines. Curves are normalized to the data. The shaded band exhibits the range of changes in shape allowed by systematic errors due to allowed variations in fragmentation function and  $\pi, K$ -decay background subtraction. For clarity it is drawn relative to the solid curve.

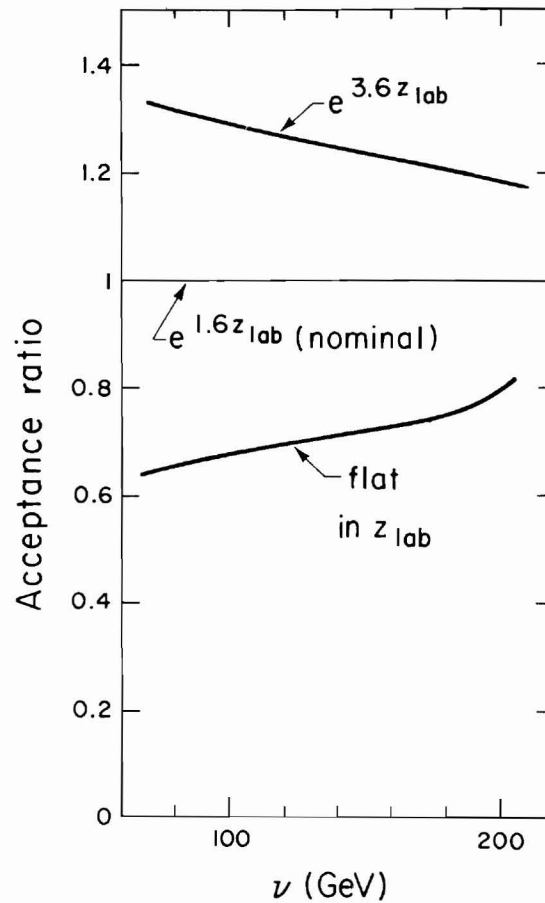


Fig. 13. Relative effect of three charmed-quark fragmentation functions upon the acceptance vs. photon energy of the EMC apparatus. The curves correspond to the nominal function and its  $\pm 1$ -standard-deviation limits allowed by the data, at the current (preliminary) analysis stage. Any additional acceptance variations caused by uncertainties in  $\pi, K$ -decay background and by other model parameters are not shown. As in the BFP analysis, model-dependence of this magnitude could mask the subtle differences in  $\nu$ -dependence arising from various choices of gluon distribution.

imposed by requiring adequate agreement with the data, for example<sup>15</sup> in the average produced muon energy at high  $\nu$ . Figures 12 (BFP) and 13 (EMC) display the changes in  $\nu$ -dependence introduced by combined uncertainties in charm fragmentation and  $\pi, K$ -decay background (Fig. 12) or in charm fragmentation alone (Fig. 13). Figure 12 also shows the changes in  $\nu$ -dependence predicted by use of various gluon distributions. At the present stage of analysis, it seems evident that the sensitivity to  $G(x)$  is seriously compromised by these systematic errors.

### III.7 Intrinsic Charm of the Nucleon?

In order to fit the observations of copious forward charm production at the ISR, Brodsky, Hoyer, Peterson, and Sakai<sup>32</sup> have proposed that, with 1% probability, the intrinsic quark content of the proton is  $uudc\bar{c}$ . The intrinsic charm component would be fast ( $\langle x_c \rangle = 2/7$ ) and would be present in addition to the evolved charm sea. In the muon data, one thereby would expect copious production of single struck charmed quarks at large  $x_{BJ}$ . No dominant contribution to  $\psi$  or fast  $c\bar{c}$  pair production would be anticipated.

For the experimental reasons discussed in section III.2, struck charmed quark model predictions for  $c(x_{BJ}) + \bar{c}(x_{BJ})$  should not be compared to measurements which correct for acceptance and branching ratio effects using the ( $\gamma$ GF) assumption that two fast charmed quarks are produced. Therefore, Fig. 11 is a potentially misleading basis for comparison of data with the intrinsic charm model. Instead, integrating over  $Q^2 > 1$  (GeV/c)<sup>2</sup> at fixed  $x_{BJ}$ , the EMC group in Fig. 14 display the cut experimental cross section  $d\sigma/dx_{BJ}$  within a kinematic region of high ( $\approx 30\%$ ) acceptance. The intrinsic-charm-model curve shown in Fig. 14 is much flatter than the  $\gamma$ GF curve. When precisely calculated, the ratio of the two curves must take into account not only the difference in  $c(x_{BJ})$  between the two models, but also the larger acceptance for (more energetic) struck quarks and the smaller number of candidates for fast  $c \rightarrow \mu X$  decay in the intrinsic charm model. Also, the charm fragmentation functions used for the two models in principle can be different; within these cuts the models are sensitive at the 20-30% level to various fragmentation choices.

Notwithstanding the potential uncertainties, intrinsic charm is predicted to dominate single extra muon production within the EMC cuts for  $x_{BJ} \gtrsim 0.3$ . The data point at  $x_{BJ} = 0.42$  lies a factor of 5 to 25 below the intrinsic charm prediction. The three events contributing to this point, after subtraction of two background events, have average effective photon energy  $\langle W^2/2M \rangle \approx 56$  GeV. Because this is far below the  $W^2$  of ISR data to which the model has been adjusted, attempts to save "intrinsic charm" have focussed on possible threshold suppression of the muon data. The calculation<sup>16</sup> which produced Fig. 14 corrects for threshold effects by using the "slow rescaling" variable  $\xi = x_{BJ}(1 + m_c^2/2M\nu x_{BJ})$  as in neutrino production of charm by means of struck light quarks. This factor does not take into account the energy needed to put the unstruck "spectator" charmed quark on shell; at  $W^2/2M = 56$  GeV it produces a negligible correction. D.P. Roy<sup>33</sup> has argued in favor of a suppression factor  $(1 - (W_{th}/W)^2)^7$ , where  $W_{th}^2 \approx 21$  GeV<sup>2</sup> at threshold. For the data point in question this amounts to a

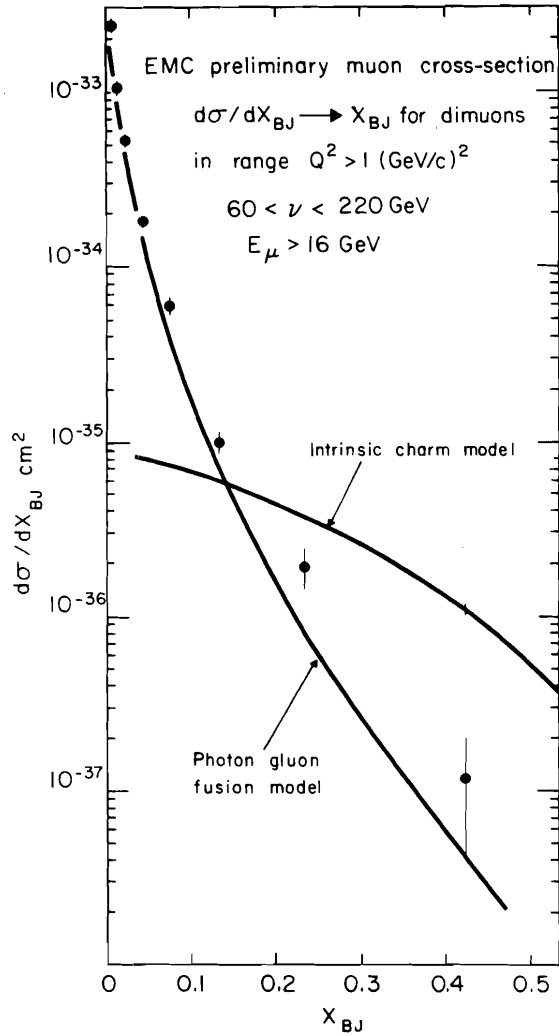


Fig. 14. Charm cross section, within indicated cuts, differential in  $x_{BJ}$ , for EMC data collected at 250 GeV. The photon-gluon fusion model is as in Fig. 11. The intrinsic charm model, as in Ref. 32, corresponds to  $uudc\bar{c}/uud = 1\%$ . After subtraction of two  $\pi, K$ -decay background events, the point at  $x_{BJ}=0.42$  represents 3 events (out of a total of 3150) with  $\langle Q^2 \rangle \approx 75$ ,  $\langle \nu \rangle \approx 95$ , effective photon energy  $\langle W^2/2M \rangle \approx 56$  GeV, and  $\approx 30\%$  acceptance within cuts. Over the range allowed by the dimuon data, different fragmentation assumptions can change the model predictions by  $\approx \pm 25\%$  in this  $x$  region. The intrinsic charm calculation uses the rescaling variable  $\xi = (Q^2 + m_c^2)/2M\nu$ . If  $m_{c\bar{c}}^2$  is used in place of  $m_c^2$ , the threshold effects can be more pronounced, possibly mitigating the disagreement between the data and the intrinsic charm model.

factor of 4.7. Brodsky<sup>34</sup> agrees that Roy's suppression factor is justified very close to threshold by counting phase space factors, but is not sure that it would apply at  $(W/W_{th})^2$  as high as 5. Using the rescaling variable  $\xi = x_{BJ}(1 + m_1^2/2Mv x_{BJ} + \bar{m}_1^2/2Mv\bar{x})$ , where  $(\bar{m}_1)^2 = m_c^2 + (\bar{k}_1)^2$ ,  $M$  is the nucleon mass, and  $\bar{x}$  is the momentum fraction of the unstruck "spectator" charmed quark, Brodsky and Peterson<sup>35</sup> have estimated the threshold suppression factor using the correlation between  $x_{BJ}$  and  $\bar{x}$  calculated in the intrinsic charm model. While somewhat dependent on choice of parameters, their factor is typically in the range 1.5-2. They also observe that  $Q^2$  evolution can introduce  $\approx 20\%$  depletion of  $c(x_{BJ})$  near  $x_{BJ}=0.4$ , relative to the unevolved charm distribution used in calculations relevant to ISR data.

To summarize, the EMC muon data appear to conflict with the intrinsic charm model by a factor of 5 to 25. The disagreement may be reducible to a factor of 2 to 10, once threshold and evolution effects are optimally taken into account. In order to rule out the model, the muon result correspondingly would need to withstand scrutiny at the factor of 2 level. Doubtless the experimenters are amply motivated to finalize and publish the details of their analysis.

#### IV. INELASTIC $\psi$ MUOPRODUCTION

##### IV.1 Background

The preceding sections of this review have concerned data which are compared only to the first of the seven diagrams in Table V. When a  $\psi$  is muoproduced in combination with additional hadrons which are not from charmonium decay, second-order calculations using the diagrams labelled "recoil quark", "three gluon", and "C<sup>-</sup> color singlet allowed" may be tested. The available data consist of early EMC results<sup>17</sup> and the final BFP results of Markiewicz *et al.*<sup>10</sup>.

In either experiment, the  $\psi$  acceptance is smaller for inelastic than for elastic production. The inelastic data, characterized by elasticity  $z \equiv E(\psi)/E(\gamma\gamma)$ , cannot be constrained by the elastic requirement  $z=1$ . The region  $z>0.9$  is heavily contaminated by feed-down of elastic events in combination with radiative corrections, both to the diagrams and to the calorimeter response. Decays to  $\psi'$  and  $\chi$  states also contribute. This region is excluded from the BFP analysis. The region  $0.7<z<0.9$  is expected to possess some contamination from  $\psi'$  production and decay into  $\psi\pi\pi$  or  $\psi\eta$ ; the detailed BFP results<sup>10</sup> are presented separately for  $z<0.7$  and  $0.7<z<0.9$ . The relevant calculations produce either lengthy expressions<sup>26</sup> or results presented primarily in graphical form<sup>21-25, 27</sup>.

Despite these complications, the analysis is important to pursue for the following reasons:

- (1) Unlike photon-gluon fusion, calculations using the second-order diagrams make predictions for distributions in the variables  $z$  and  $p_1$ . In contrast to  $c \rightarrow \mu\nu X$  muoproduction, these variables are measurable. Broadening of the observed  $p_1$  distribution by gluon emission should be observable.
- (2) A question of principle, relevant to future QCD calculations, is answerable:

For production of a specific  $Q\bar{Q}$  bound state, is it necessary that color and C-parity quantum numbers be conserved? If so, the "recoil quark" and "three gluon" diagrams should be excluded<sup>26</sup>.

(3) For the three diagrams capable of producing the  $c\bar{c}$  pair in a  $1^-$  color singlet, it is unnecessary to invoke "semilocal duality" in order to restrict the calculation to  $\psi$  production: a normalized  $\psi$  wavefunction can be used<sup>26</sup>.

(4) For the same three diagrams, restricting  $z < 0.9$  forces both gluons far off shell<sup>26</sup>. This removes the philosophical shortcomings characteristic of  $\gamma\text{GF}$  (section III.5).

#### IV.2 General Features of the Data

From BFP data<sup>10</sup>, the inelastic  $\psi$  muoproduction cross section at 209 GeV is  $0.14 \pm 0.01 \pm 0.02$  nb for  $z < 0.7$ , and  $0.14 \pm 0.01 \pm 0.03$  nb for  $z > 0.7$ . The total, including contamination from  $\psi'$  and  $\chi$  decay to  $\psi$ , is  $0.28 \pm 0.03 \pm 0.05$  nb. The total (elastic + inelastic)  $\psi$  muoproduction cross section is  $0.64 \pm 0.03 \pm 0.10$  nb.

Distributions of BFP data<sup>10</sup> in the angular variables  $|\cos\theta|$  and  $\phi_F$  (section III.2) are similar to the elastic results (Fig. 7) for  $0.7 < z < 0.9$ , and are consistent with being flat when  $z < 0.7$ .

Figure 15 recalls the  $t$  distribution of elastic  $\psi$  muoproduction. The correction for the coherent component, unseparated by BFP data, is shown in part (a) of that Figure. The fit effective slope  $b_{\text{eff}} = d \ln \sigma / dt(t=0)$  of the incoherent component is  $(2.56 \pm 0.34 \pm 0.2) (\text{GeV}/c)^{-2}$ . Figure 16 displays the much broader  $t$  distribution of BFP inelastic  $\psi$  muoproduction data in both  $z$  regions. The effective slopes are approximately half the elastic value (see caption). This confirms the original EMC observation<sup>17</sup> of a much flatter  $t$  distribution for inelastic  $\psi$  production, in agreement with predictions using the second-order diagrams, when compared to elastic  $\psi$  production.

The  $Q^2$  distribution of the effective cross section for inelastic- $\psi$  virtual photoproduction is exhibited (a) for two  $z$  regions and (b) for the combined BFP sample in Fig. 17. The propagator mass fit to the combined sample is  $\Lambda = 3.0 \pm 0.2$  GeV/ $c^2$ , in agreement with  $\psi$  dominance. The calculation of Duke and Owens<sup>23</sup>, using all second-order diagrams and invoking semilocal duality, is also in reasonable agreement. Details of the (unpublished) Keung "color singlet" calculation<sup>27</sup>, with which the data are in less satisfactory agreement, are not yet available.

#### IV.3 Must the Diagrams Conserve Color?

The shapes of BFP distributions in photon energy  $E_\gamma$  (Fig. 18(a)) and in elasticity  $z$  (Fig. 18(b)) unequivocally settle this question in the affirmative. In each case the semilocal duality calculation<sup>23,24</sup> of Duke and Owens, using both color-conserving and nonconserving graphs, rises far more steeply than the data. If the color-nonconserving graphs are excluded, and semilocal duality revoked in favor of a specific  $\psi$  wavefunction, the  $\gamma g \rightarrow \psi g$  calculation of Berger and Jones<sup>26</sup> is a reasonable description of the data. It should be noted that the former calculation has not been cut at  $z < 0.9$  for comparison to the data in Fig. 18(a);

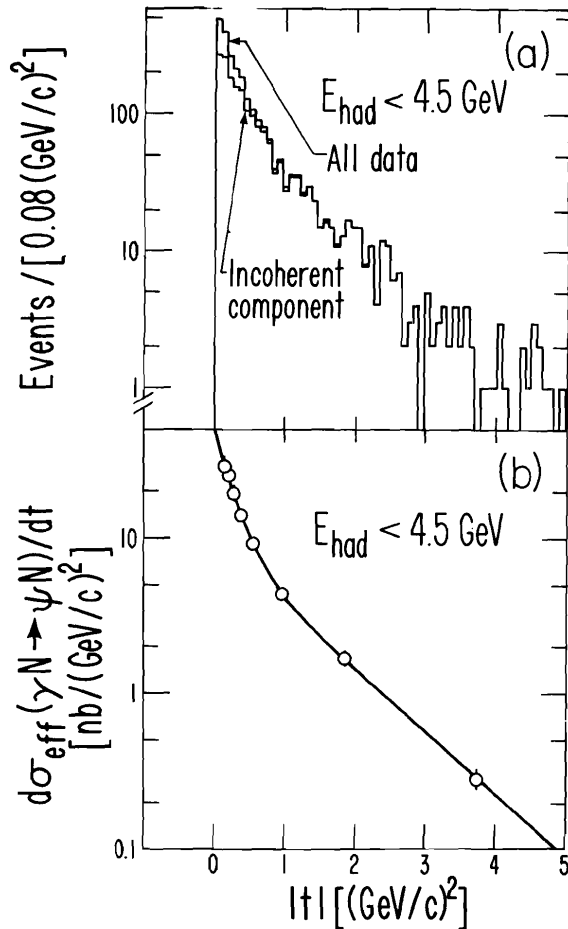


Fig. 15. Dependence on  $t$  (BFP data) of the effective cross section for the reaction  $\gamma\gamma Fe \rightarrow \psi X$  (energy of  $X < 4.5$  GeV). (a) Events in the  $\psi$  mass range  $-0.052 < \log_{10}(m_{\mu+\mu-}/3.1) < 0.052$  vs. measured  $t$ , defined as  $t_{min} + (p_{\perp}^2)_{\psi}$ . The upper histogram is all data; the lower is that portion of the data ascribed to incoherent production  $\gamma\gamma N \rightarrow \psi N$ . (b) Incoherent contribution, corrected for all experimental effects, vs.  $t$  with resolution unfolded. The curve is proportional to  $0.815\exp(4.3t) + 0.185\exp(0.9t)$ , with an effective slope parameter  $d \ln \sigma / dt(t=0) = (2.56 \pm 0.34 \pm 0.2) (\text{GeV}/c)^{-2}$ . Errors are statistical, including the error introduced by subtracting the coherent component of the cross section.

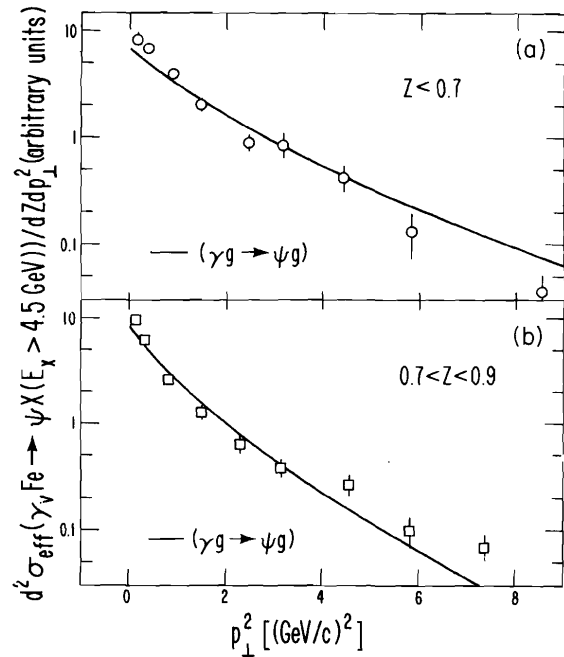


Fig. 16. Dependence on  $p_{\perp}^2$  (BFP data) of the effective cross section for the reaction  $\gamma\gamma Fe \rightarrow \psi X$  (energy of  $X > 4.5$  GeV). [When measured with respect to the  $\gamma_{\nu}$  momentum,  $p_{\perp}^2$  (of the  $\psi$ ) is essentially the same for elastic data as  $-t$ , in this photon energy range.] Data are divided into two regions of  $z = E(\psi)/E(\gamma_{\nu})$ . The solid curve is the "color singlet"  $\gamma g \rightarrow \psi g$  calculation (Ref. 26) arbitrarily normalized to the data. For  $z < 0.7$  ( $0.7 < z < 0.9$ ),  $b_{eff}$  is  $1.02 \pm 0.25$  ( $1.54 \pm 0.11$ )  $(\text{GeV}/c)^{-2}$ , roughly half the elastic value (Fig. 15).

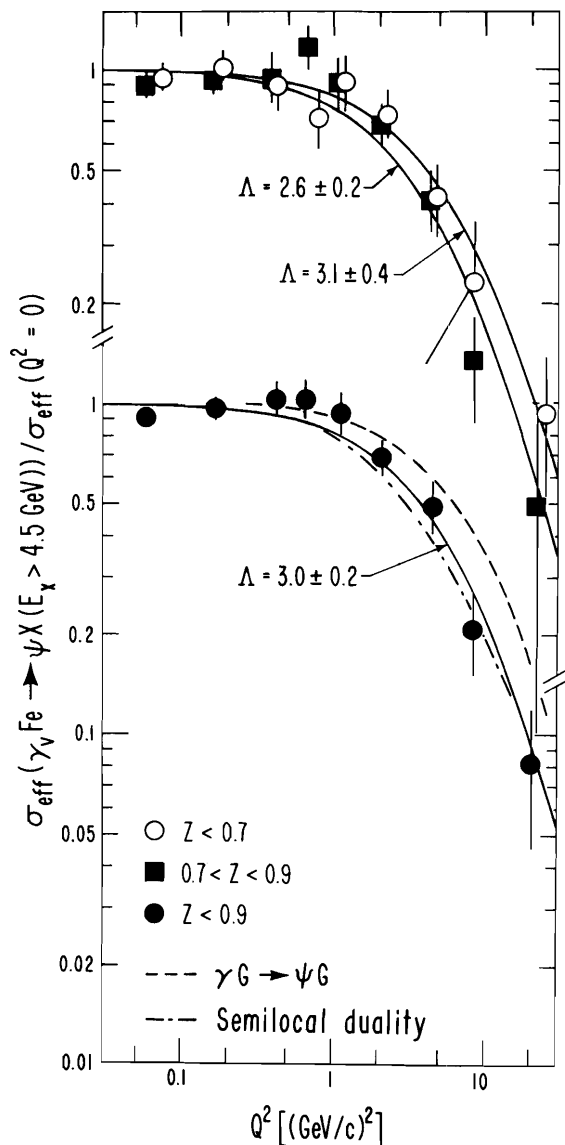


Fig. 17. Dependence upon  $Q^2$  of the effective cross section for the reaction  $\gamma\gamma\text{Fe} \rightarrow \psi X$  (energy of  $X > 4.5$  GeV), normalized to unity at  $Q^2=0$ . BFP data with statistical errors are presented for the elasticity regions  $z < 0.7$  (open circles),  $0.7 < z < 0.9$  (filled squares), and  $z < 0.9$  (filled circles). Fits to  $(1+Q^2/\Lambda^2)^{-2}$  are shown by solid lines, with the fit values of  $\Lambda$  indicated in (GeV/c). The dashed line is the "color singlet"  $\gamma G \rightarrow \psi G$  calculation of Keung (Ref. 27); the dot-dashed line is the "semilocal duality" calculation of Duke & Owens (Ref. 23).

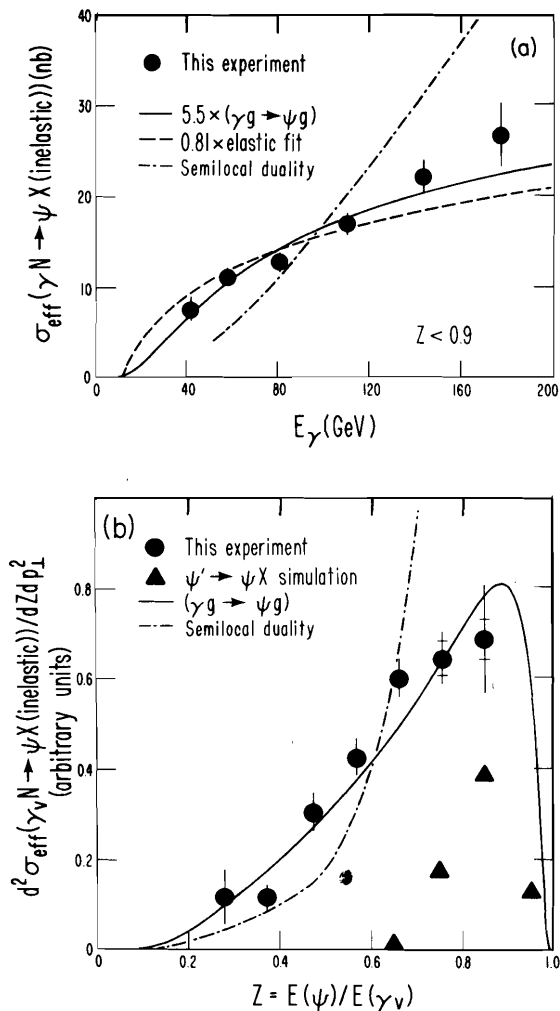


Fig. 18. Dependence upon (a) photon energy  $E_\gamma$  and (b) elasticity  $z$  of the effective cross section for the reaction  $\gamma\gamma N \rightarrow \psi X$  (energy of  $X > 4.5$  GeV). BFP data with statistical errors are shown as filled circles; outer error flags in (b) include uncertainties in corrections for feed-down of elastic events. Filled triangles in (b) represent twice the  $\psi' \rightarrow \psi X$  contribution expected from Ref. 9. Solid curves are the "color singlet"  $\gamma G \rightarrow \psi G$  calculation of Berger and Jones (Ref. 26); dot-dashed curves are the "semilocal duality" calculation of Duke and Owens (Refs. 23, 24); the dashed curve fits the  $E_\gamma$ -dependence of the elastic data [Fig. 9(a)]. Curves in (b) are arbitrarily normalized to the data.

however, the measured<sup>10</sup> dependence upon  $E_\gamma$  of data with  $z < 0.7$  and  $0.7 < z < 0.9$  shows no strong variation with  $z$ . The points in Fig. 18(a) are listed in Table VII.

Unfortunately, the triumph of the color-conserving diagrams is incomplete: they account for only 18% of the observed cross section (Table VII), if  $\alpha_s = 0.3$  is used<sup>26</sup>.

#### IV.4 Summary

The color-conserving second-order diagrams represent the inelastic- $\psi$  muoproduction data in shape but not in absolute normalization. If the factor of 5.5 in normalization can be found, phenomenologists will be able to extract the gluon  $x$  distribution from BFP data<sup>26</sup> now in final form.

#### V. FUTURE PROSPECTS

The BFP experiment consisted of one run in the first half of 1978 using the now-extinct Fermilab muon beam. Its multimMuon analyses, defined by the publication<sup>15</sup> or submission for publication<sup>5,10</sup> of three Ph.D. dissertations, are complete. The EMC experiment and multimMuon analyses continue, with newer results to be expected in all areas covered by this review. Further EMC running with the STAC target is not now foreseen.

A subset of the BFP collaboration are approved<sup>36</sup> to operate an improved spectrometer in a new Fermilab muon beam at  $\approx 3$  times higher energy. Beam construction is projected to reach full force by 1983, with new data available possibly by 1985. These plans depend critically on the prospects for U.S. government support of basic research.

#### VI. ACKNOWLEDGEMENTS

I am grateful to F. Brasse, E. Gabathuler, C. Gössling, and T. Sloan of EMC; J. Feltse of BCDMS; and J. Butler of Fermilab-Illinois for care and patience in explaining to me their experimental results. It is a pleasure to recognize the present and past collaboration of my BFP colleagues, particularly T. Markiewicz, whose heroic Ph.D. thesis is a major input to this review.

The author has been supported by the Director, Office of Energy Research, Office of High Energy and Nuclear Physics, High Energy Physics Division of the U.S. Department of Energy under Contract No. W-7405-ENG-48.

#### REFERENCES

- (1) Clark, A.R., K.J. Johnson, L.T. Kerth, S.C. Loken, T.W. Markiewicz, P.D. Meyers, W.H. Smith, M. Strovink, W.A. Wenzel, R.P. Johnson, C. Moore, M. Mugge, R.E. Shafer, G.D. Gollin, F.C. Shoemaker, and P. Surko, Phys. Rev. Lett. 45 (1980) 686.

- (2) Clark, A.R., et al., Phys. Rev. Lett. 46 (1981) 299.
- (3) Aubert, J.J. et al. [CERN-DESY (Hamburg)-Freiburg-Kiel-Lancaster-LAPP (Annecy)-Liverpool-Oxford-Rutherford-Sheffield-Turin-Wuppertal collaboration], Observation of Wrong-Sign Tri-Muon Events in 250 GeV Muon-Nucleon Interactions, CERN, CERN/EP 81-87 (August 1981), submitted to Physics Letters.
- (4) Bollini, D., et al., Production of Muons by Virtual Photons and Upper Limit for Upsilon Production, CERN, CERN/EP 81- (August 1981).
- (5) Smith, W.H., et al., Study of Rare Processes Induced by 209-GeV Muons, Univ. of California, Berkeley, LBL-12789 (May 1981), submitted to Phys. Rev. D.
- (6) Clark, A.R. et al., Phys. Rev. Lett. 43 (1979) 187.
- (7) Aubert, J.J., et al., Phys. Lett. 89B (1980) 267.
- (8) Clark, A.R., et al., Phys. Rev. Lett. 45 (1980) 2092.
- (9) Binkley, M., et al., J/ $\psi$  Photoproduction from 60 to 300 GeV/c, paper No. 58 submitted to Bonn conference (1981); Butler, J., private communication.
- (10) Markiewicz, T.W., et al., Muoproduction of J/ $\psi$  (3100), Univ. of California, Berkeley, LBL- (October 1981), to be submitted to Phys. Rev. D.
- (11) Aubert, J.J., et al., Phys. Lett. 94B (1980) 96.
- (12) Aubert, J.J., et al., Phys. Lett. 94B (1980) 101.
- (13) Clark, A.R., et al., Phys. Rev. Lett. 45 (1980) 682.
- (14) Clark, A.R., et al., Phys. Rev. Lett. 45 (1980) 1465.
- (15) Gollin, G.D., et al., Phys. Rev. D24 (1981) 55.
- (16) Best, C.H., et al., New Results on Multi-Muon Production in 250 GeV  $\mu^+$ Fe Interactions, Rutherford Lab., RL-81-044 (May 1981); Coignet, G., talk at European Physical Society International Conference (Lisbon, 9-15 July, 1981); European Muon Collaboration, private communication.
- (17) Aubert, J.J., et al., Inelastic J/ $\psi$  Production in 280 GeV Muon-Iron Interactions, CERN, CERN/EP 80-84 (June 1980), submitted to Phys. Lett.; Mount, R.P., et al., in High Energy Physics-1980 (Proceedings of the XX International Conference on High Energy Physics, Madison, Wisconsin, 1980), L. Durand and L.G. Pondrom, eds. (American Institute of Physics, New York, 1981) 205. Some of the results reported here are in serious disagreement with those of Ref. 10. The  $Q^2$ -dependence of the effective photon cross section is reported as  $(1+Q^2/\Lambda^2)^{-2}$  with  $\Lambda=1.8\pm 0.2$  GeV/c; Ref. 10 obtains  $\Lambda=3.0\pm 0.2$ . The  $\nu$ -dependence is reported to be much steeper than in Ref. 10.
- (18) Weiler, T., Phys. Rev. Lett. 44 (1980) 304.
- (19) Barger, V., W.Y. Keung, and R.J.N. Phillips, Phys. Lett. 91B (1980) 253.
- (20) Leveille, J., and T. Weiler, Azimuthal Dependence of Diffractive  $\psi$  and  $D\bar{D}$  Muoproduction and a Test of Gluon Spin, Parity, and  $k_{\perp}$ , Northeastern Univ., NUB #2479 (1980), submitted to Phys. Rev. D.
- (21) Leveille, J., and T. Weiler, Phys. Lett. 86B (1978) 377.
- (22) Duke, D.W., and J.F. Owens, Phys. Lett. 96B (1980) 184.
- (23) Duke, D.W., and J.F. Owens, Phys. Rev. D23 (1981) 1671.
- (24) Duke, D.W., and J.F. Owens, Phys. Rev. D24 (1981) 1403.
- (25) Tajima, T., and T. Watanabe, Phys. Rev. D23 (1981) 1517.
- (26) Berger, E.L., and D. Jones, Phys. Rev. D23 (1981) 1521.
- (27) Keung, W.Y., Inclusive Quarkonium Production, Brookhaven National Lab., written version of talk delivered at Z<sup>0</sup> Physics Workshop, Cornell University (February 1981).
- (28) Camerini, U., et al., Phys. Rev. Lett. 35 (1975) 483.
- (29) Ellis, J., in Weak Interactions - Present and Future (Proceedings of the SLAC Summer Institute on Particle Physics, SLAC, July 10-21, 1978), M.C. Zipf, ed. (SLAC, Stanford, 1978) 69.
- (30) Glück, M., E. Hoffmann, and E. Reya, Univ. of Dortmund, DO-TH 80/13 (1980).
- (31) Phillips, R.J.N., in High Energy Physics-1980 (Proceedings of the XX International Conference on High Energy Physics, Madison, Wisconsin, 1980), L. Durand and L.G. Pondrom, eds. (American Institute of Physics, New York, 1981) 1471.
- (32) Brodsky, S.J., P. Hoyer, C. Peterson, and N. Sakai, Phys. Lett. 93B (1980) 451.
- (33) Roy, D.P., private communication, and discussion following talk of J. Drees, Bonn conference (1981).
- (34) Brodsky, S.J., private communication.
- (35) Brodsky, S.J., and C. Peterson, On the Measurement of the Intrinsic Charm Sea Deep Inelastic Leptoproduction, SLAC, informal note privately communicated (October 1981).
- (36) Loken, S.C., et al., Fermilab Proposal 640 (1980).

DISCUSSION

N.W. Reay, Ohio State University: Questions concerning intrinsic charm:

1. A Fermilab-Rochester group reported a limit of 1/20% (0.0005) on the intrinsic  $c\bar{c}$  charm at the Gordon Conference. Does anyone from that experiment care to comment?
2. Summing two runs of the Fermilab Neutrino Experiment E-531 should yield roughly 2000 neutral current events. If the intrinsic charm model is true, does anyone care to comment on how many charmed particles we should see?

No answers.

R.D. Sard, University of Illinois: I should like to address a simple question to the theorists. Is it possible to produce even-parity  $c\bar{c}$  states, such as  $\chi$ , in electro-production?

E.L. Berger, ANL: Yes, but the production is suppressed because too many gluons are required to satisfy both color and spin-parity requirements.